Colloids and Surfaces A: Physicochemical and Engineering Aspects 736 (2026) 139621

Contents lists available at ScienceDirect

Colloids and Surfaces A: Physicochemical and Engineering Aspects

journal homepage: www.elsevier.com/locate/colsurfa

Rheology and interaction mechanisms of polyelectrolyte-wormlike micellar surfactant complexes: A two-dimensional correlation spectroscopy and time-concentration superposition study

Duccio Tatini [a,b,*], Alberto Fidi [c], Mert Acar [b,d], Pierandrea Lo Nostro [b,d]

[a] Department of Biotechnologies, Chemistry and Pharmacy, University of Siena, Siena 53100, Italy
[b] Centre for Colloid and Surface Science (CSGI), University of Florence, Via della Lastruccia 3, Sesto Fiorentino 50019, Italy
[c] Polymer Chemistry and Materials, KU Leuven, Celestijnenlaan 200J - box 2404, Leuven 3001, Belgium
[d] Department of Chemistry "Ugo Schiff", University of Florence, Sesto Fiorentino 50019, Italy

HIGHLIGHTS

- Polyelectrolyte charge controls supramolecular aggregation with oleate micelles.
- ε-poly-L-lysine induces coacervate-like structuring affecting rheological behavior.
- Poly(acrylic acid) enhances viscoelasticity via hydrogen-bonding interactions.
- Two-dimensional correlation spectroscopy elucidates distinct binding pathways.
- Time–concentration superposition provides predictive rheological scaling.

GRAPHICAL ABSTRACT

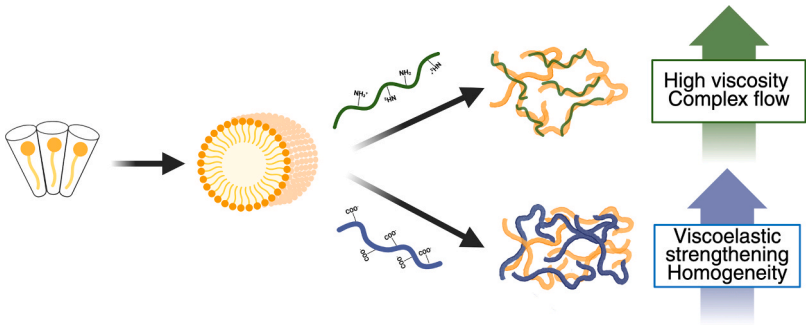

ARTICLE INFO

Keywords:
Catanionic interactions
Potassium oleate
Concentration scaling
Confocal microscopy
Non-Newtonian fluids
Viscoelasticity
Two-dimensional correlation spectroscopy

ABSTRACT

This study investigates the rheological behavior and molecular interaction mechanism of polyelectrolyte–wormlike micellar complexes formed by potassium oleate (KOL) with either ε-poly-L-lysine (PL) or poly(acrylic acid) (PAA) in water. Steady shear and oscillatory rheology experiments, combined with confocal laser scanning microscopy (CLSM), were performed to evaluate the effect of polyelectrolyte charge and concentration on the micellar organization. In KOL–PL systems, a critical PL concentration (≈1.5 %) triggered a sharp viscosity increase and complex flow behavior, associated with the formation of supramolecular or coacervate-like aggregates. CLSM confirmed the appearance of structured domains at high PL content. By contrast, KOL–PAA mixtures exhibited a progressive increase in viscosity and viscoelastic moduli upon PAA addition although no aggregate could be detected by visual inspection, suggesting the onset of rearrangements at the nanoscale. Two-dimensional correlation spectroscopy (2D-COS) of attenuated total reflection Fourier-transform infrared (ATR-FTIR) data revealed distinct interaction pathways: in KOL–PL the carboxylate headgroups are the most sensitive moieties to polyelectrolyte addition, followed by alkyl tails and hydration water, consistently with a direct electrostatic binding. In KOL–PAA, the first response occurred in the hydration layer and hydrogen-bonding environment before reaching the micellar headgroups and cores, suggesting an

* Correspondence to: Via Aldo Moro, 2, Siena 53100, Italy.
E-mail address: duccio.tatini@unisi.it (D. Tatini).

https://doi.org/10.1016/j.colsurfa.2026.139621
Received 5 November 2025; Received in revised form 11 January 2026; Accepted 18 January 2026
Available online 22 January 2026

interaction mechanism mediated by counterions and hydrogen bonds. Finally, a time–cosolute concentration superposition (TCCS) approach was successfully applied to the rheological data of both systems to obtain unified master curves and scaling laws, demonstrating its predictive value for polyelectrolyte–micelle complexes.

1. Introduction

Understanding the rheological properties of complex fluids, such as wormlike micelles and polyelectrolyte mixed systems is of paramount importance for industrial and biological applications [1–4]. These systems are characterized by a multifaceted self-assembly behavior and exhibit unique rheological features that have intrigued scientists for decades [5].

Wormlike micelles (WLMs) originate from the self-assembly of amphiphilic molecules under specific conditions in solution (surfactant aggregate curvature, temperature, pH, surface charge, presence of salts or other cosolutes), and possess a unique structure resembling elongated threads or worms [6–9]. Their rheological properties are regulated by a delicate balance between entanglement, hydrodynamic interactions, and breaking and reforming of micellar structures [10]. This delicate interplay results in peculiar rheological properties, such as shear-thinning and viscoelasticity, that can be finely modulated in response to external stimuli or environmental changes [11–14]. WLMs constitute a paradigmatic class of complex fluids, as their linear viscoelastic response directly reflects the dynamics and connectivity of the entangled micellar network at mesoscopic length scales. Small-amplitude oscillatory shear measurements have been extensively employed to relate macroscopic rheological properties, such as viscosity and relaxation time, to micellar growth, breaking, and entanglement processes [15]. More advanced approaches including nonlinear rheology, large-amplitude oscillatory shear and recovery-based protocols can provide complementary insight into micellar restructuring and stress relaxation beyond the linear regime [16].

Polyelectrolyte complexes (PEC) are multifunctional systems obtained via complexation between oppositely charged polyelectrolytes, leading to the formation of materials with distinctive physicochemical properties and phase behavior [17–19]. These complexes can self-assemble into different architectures at the nanoscale, resulting in highly stable structures due to strong electrostatic interactions, and making PECs resistant to environmental changes such as pH and ionic strength [20–22]. This stability, combined with their biocompatibility and tunable properties, makes PECs particularly attractive for a variety of applications, including drug delivery systems [23], water treatments [24], and as components in responsive materials [25,26].

A special case is represented by polyelectrolyte surfactant complexes (PESCs), a class of highly ordered supramolecular materials obtained through the combination of polyelectrolytes and ionic surfactants [27–29]. These materials take advantage of the individual properties of charged polymers (mechanical strength and stability) and surfactants (ability to self-assemble in lyotropic mesophases) to reach a synergistic effect on the rheological and phase behavior [30].

PESCs find several interesting applications as detergents, personal care products, pharmaceutical formulations and responsive materials, thanks to the possibility of modulating their physicochemical and mechanical properties by modifying the charge ratio, the concentration, or chemical environment (temperature, ionic strength, pH) [31,32].

When wormlike micelles and polyelectrolytes interact in solution, interesting phenomena can occur due to the complex interplay between their structures and charges [33,34]. These interactions can greatly influence the rheological properties of the solution, including its viscosity, elasticity, and flow behavior [35].

The interaction between wormlike micelles and neutral or oppositely charged polymers has been extensively investigated, showing that polymer adsorption, bridging, or complexation play a key role in modulating the overall systems' response [36–39]. In contrast, the interaction between wormlike micelles and polymers bearing the same net charge has received far less attention and is generally expected to be weak or absent due to electrostatic repulsion. As a result, synergistic effects between polyelectrolytes and wormlike micellar systems with the same charge are generally overlooked. The present study provides, to the best of our knowledge, the first experimental evidence of a strong cooperative interaction between an anionic wormlike micellar system and a negatively charged polyelectrolyte, leading to a pronounced enhancement of viscosity and viscoelasticity despite the unfavorable electrostatic conditions.

Previous works demonstrated that sodium and potassium oleate can self-assemble into rodlike or wormlike micelles at moderately high concentration in aqueous dispersion. The self-assembly behavior of oleate salts is intriguingly interesting as it offers a wide set of different structures depending on the pH and thus on the charge of the monomers. The viscoelastic properties of these systems are determined by a number of different parameters like temperature, pH, nature and concentration of added salts [40–42]. In this work we explore the rheological behavior and the interaction mechanism of two polyelectrolyte surfactant complexes based on potassium oleate (KOL) in the presence of different charged polymers. In one case we added ε-poly-L-lysine (PL), a biopolymer consisting of approximately 25–35 L-lysine residues connected by a peptide bond between the carboxylic group and the ε-amino moiety [43]. In solution, under neutral or acidic pH conditions PL exists in a polycationic form due to the protonation of the amino groups in α position [44]. PL is widely used as food preservative, antimicrobial, antifungal and emulsifying agent, in hydrogels, drug-delivery systems and biodegradable materials [45]. In the second system, a low-molecular weight polyacrylic acid (PAA) was added to the KOL dispersion. PAA is a synthetic polymer derived from the polymerization of acrylic acid: in neutral conditions PAA is an anionic polymer, since the carboxylic groups located on the side chains are partially or fully deprotonated [46,47]. PAA shows a high solubility in water and an excellent ability to form hydrogel, along with remarkable dispersant, thickening, and stabilizing properties. For a comprehensive account on the state-of-the-art of the current applications of PAA the readers can refer to the vast literature, e.g. references [48–50].

The flow behavior and the viscoelastic properties of KOL-PL and KOL-PAA complexes were investigated by means of flow curves experiments and oscillatory measurements, in order to elucidate the effect of the cosolute (i.e., the polyelectrolyte) charge and concentration on the overall rheological and phase behavior. In addition to rheological analysis, structural insights were obtained through confocal laser scanning microscopy (CLSM), to visualize the micellar network and identify morphological transitions induced by polyelectrolyte addition. By correlating CLSM data with the macroscopic flow behavior, we elucidated the role of aggregation and phase separation phenomena in shaping the rheological response of the mixed systems. To get a deeper insight into the interaction mechanism between the surfactant and polyelectrolyte molecules, two-dimensional correlation spectroscopy (2D-COS) was employed. Initially developed for infrared spectroscopy, the application of 2D-COS has been extended to a wide range of analytical techniques—from Raman and NMR to non-spectroscopic methods like chromatography—and external perturbations, including temperature, pressure, and pH [51–53]. This versatility made 2D-COS a powerful tool for the analysis of different samples ranging from polymers, surfactants and polyelectrolytes to complex biological, pharmaceutical, agrifood and environmental systems [54–59]. In this work, 2D-COS was applied to the concentration-dependent attenuated total reflection Fourier-transform infrared (ATR-FTIR) spectra to investigate

the specific interaction pathways within the KOL-PL and KOL-PAA systems and determine the sequence of molecular-level rearrangements occurring upon polyelectrolyte addition. The 2D-COS data were directly correlated with the results obtained from the rheological analysis since oscillatory and steady-state measurements describe the collective response of the system to deformation, reflecting changes in micellar entanglement and network dynamics that are not directly accessible through spectroscopy alone. By combining rheology with 2D-COS a direct link between molecular-level interactions and the macroscopic viscoelastic response can be established, enabling a mechanistic interpretation of the complexation processes modulating the behavior of the oleate-based wormlike micellar systems.

Moreover, an important methodological aspect of this study concerns the application of time–cosolute concentration superposition (TCCS) approach to predict the concentration scaling of shear viscosity and viscoelastic properties, like the *plateau* modulus and relaxation times. While superposition principles are well established in polymer rheology and have been sporadically extended to selected colloidal systems, their applicability to complex fluids formed by surfactant–polyelectrolyte mixtures remains largely unexplored [60]. In a recent work, a time–concentration superposition method was successfully applied to experimental oscillatory data for studying the concentration scaling properties of viscoelastic polymer solutions [61]. Wang and coworkers demonstrated the validity of the time-concentration superposition concept to estimate the concentration scaling exponents of linear viscoelastic properties for different colloidal dispersions and liquid crystalline polymer solutions [62]. In wormlike micelles-polyelectrolyte complexes multiple dynamic processes like micellar breaking and recombination, entanglement, polymer-mediated interactions, electrostatic effects coexist and may, in principle, hinder the validity of superposition approaches. Demonstrating that TCCS can successfully collapse steady shear and oscillatory rheological data in these systems represents a significant advancement, providing a predictive framework to describe the concentration-dependent rheological behavior. In this work, we extended the validity of TCCS approach to the case of polyelectrolyte surfactant complexes.

2. Materials and methods

2.1. Materials

Potassium oleate (>99 %, Sigma-Aldrich, Milan, Italy), ε-poly-L-lysine (PL) (M_w = 3500–4500 Da, Sigma-Aldrich, Milan, Italy) and poly (acrylic acid, sodium salt) solution (M_w = 1200 g/mol, 45 % w/w in water, Aldrich, Milan, Italy) were used as received without any further purification. All solutions and dispersions were freshly prepared with deionized Milli-Q water (resistivity > 18 MΩ·cm at 25 °C).

2.2. Sample preparation

The samples containing PL were prepared by adding a weighted amount of KOL to water solutions of PL at different concentrations (1, 1.5, 2, 2.5, 3 % w/w) under constant magnetic stirring at approximately 600 rpm for 1 h at room temperature. The final concentration of KOL was 10.7 % w/w in all the samples.

In the case of PAA, the 45 % w/w water solution was diluted to reach different final PAA concentrations (1.5, 2.4, 3.6 and 4.8 % w/w), then a weighted amount of KOL was added under constant magnetic stirring at approximately 600 rpm for 1 h at room temperature. The final surfactant concentration was 10.7 % w/w in all the samples. The pH of the formulations was measured by a 744 pH-meter equipped with a combined LLWOC microelectrode (Metrohm Italiana, Italy): for all the samples the pH was 8.0 ± 0.1, and this value did not change over the time required for the rheology experiments. In these pH conditions the fraction of protonated amino groups on each PL chain is about 30 %, while in the case of PAA the carboxylate side groups are essentially all deprotonated.

2.3. Rheology measurements

The rheology experiments were performed on a Paar Physica UDS 200 rheometer, using a cone-plate geometry (40 mm, 2°), in controlled-stress mode. The temperature was controlled by a Peltier plate system and fixed at 25°C. For the frequency sweep measurements, the storage G' and loss G'' moduli were measured over the frequency range comprised between 10^{-3} and 10^{2} Hz. The linear viscoelastic region was determined by preliminary amplitude sweep tests and the strain value was fixed at 1 % for all experiments. The flow curves were acquired by applying a torque in the range between 10^{-1} and $5{\cdot}10^{3}$ mN·m. All the experiments were repeated at least three times, and silicone oil was applied around the geometry to prevent water evaporation from the sample. For KOL–PL systems the storage and loss moduli exhibited large fluctuations between independent runs, exceeding the instrumental uncertainty. Moreover, no well-defined viscoelastic behavior and reproducible G′–G″ crossover could be identified within the investigated frequency range, despite systematic variation of strain amplitude, equilibration time, and measurement duration. For this reason the results are not presented in this work. For the time-cosolute concentration superposition procedure the rheological data were analyzed via in-house MATLAB© scripts, which are available upon request.

2.4. Confocal laser scanning microscopy (CLSM)

Confocal microscopy images were obtained using a Leica TCS SP8 laser scanning microscope (Leica Microsystems GmbH, Wetzlar, Germany), with 20 × /0.75 dry and 63 × /1.20 water objectives (Zeiss). The samples were stained with Nile Red. An argon ion laser source was used for the excitation wavelength of 514 nm, and the fluorescence emission was detected by photomultiplier tube (PMT) detectors set to a range of 600–640 nm. Image analysis was performed using Fiji software [63]. Selected CLSM images were converted to 8-bit grayscale and processed by applying an intensity threshold followed by noise-reduction steps to obtain binary black-and-white images. Particle analysis was then applied to identify pore-like features and aggregated structures within the sample and determine their projected areas.

2.5. Attenuated total reflection fourier-transform infrared spectroscopy (ATR-FTIR)

Infrared spectra were obtained in a wavenumber range of 1000–4000 cm^{-1} in attenuated total reflection (ATR) mode using a Thermo Nicolet Nexus 870 spectrometer equipped with an MCT detector (Monza, Italy). Each spectrum was averaged over 128 scans and has a spectral resolution of 2 cm^{-1}. After acquisition an offset normalization was applied and the spectra were smoothed using an eleven-point Savitzky-Golay function.

2.6. Two-dimensional correlation spectroscopy (2D-COS)

Two-dimensional correlation spectroscopy (2D-COS) was used to analyze the spectral variations in the ATR-FTIR data as a function of polymer concentration. The set of concentration-dependent spectra for each system was processed using the generalized 2D-COS algorithm developed by Noda [64,65], with the average spectrum of the series serving as the reference. The increasing polymer concentration was used as the external perturbation. This analysis generated synchronous (Φ) and asynchronous (Ψ) correlation maps, which display the in-phase and out-of-phase spectral changes, respectively. The order of responsiveness of the different molecular groups to the perturbation was then determined by interpreting the signs of the cross-peaks in both maps according to Noda's rules [66,67]. The analysis was performed using the 2DShige program (2DShige, version 1.3 © Shigeaki Morita, Kwansei-Gakuin University, 2004–2005).

3. Results and discussion

3.1. KOL-PL system

Fig. 1 shows the flow curves obtained for the KOL-PL samples at different PL concentrations.

All the samples show a shear-thinning behavior, with a Newtonian plateau followed by a steep decrease in the viscosity as the shear rate increases. The viscosity drop is more pronounced when the PL concentration is greater than 2 %. The samples at 2.5 and 3 % exhibit an interesting behavior: while the Newtonian *plateau* is still distinguishable at low shear rates, in the shear-thinning region the flow curve shows two different power-law dependencies. In the shear rate range between ~0.005 and ~10 s^{-1} the slope (obtained by linear regression) of the curve is −0.37 and −0.41 for the sample containing PL at 2.5 and 3 %, respectively. In the high shear range the slope values are −0.78 and −0.77, respectively, which are close to the value of −0.87 extrapolated for the sample containing PL 2 %.

In the PL concentration range comprised between 0 % and 2 % the flow curves were fitted according to the Cross model to obtain the zero-shear viscosity η_0, an estimate of the shear relaxation exponent, m, and the consistency index C [41,68]:

$$\eta = \eta_\infty + \frac{\eta_0 - \eta_\infty}{1 + (C\dot{\gamma})^m} \quad (1)$$

Where η_∞ is infinite shear viscosity and $\dot{\gamma}$ is the shear stress. The resulting parameters are listed in Table 1.

The zero-shear viscosity and the consistency index progressively increase with increasing PL concentration, suggesting the formation of aggregated catanionic structures, due to the strengthening of the electrostatic interactions between the positively charged aminoacidic residues on PL and the carboxylic moieties of KOL molecules. The effect induced by PL is similar to that observed upon the addition of inorganic salts to sodium and potassium oleate-based rodlike and wormlike micellar systems [41,42]: a progressive exchange between K^+ and PL molecules at the surfactant micellar interface promotes the elongation of KOL micelles and the consequent entanglement of the catanionic structures, resulting in an increased viscosity.

For comparison, a 3 % PL aqueous solution shows a nearly Newtonian flow behavior, with viscosity values one order of magnitude lower than those of the corresponding KOL–PL mixtures (see Figure S1 in the Supplementary Material), confirming that the viscosity enhancement originates from the interaction between PL and the KOL micellar network.

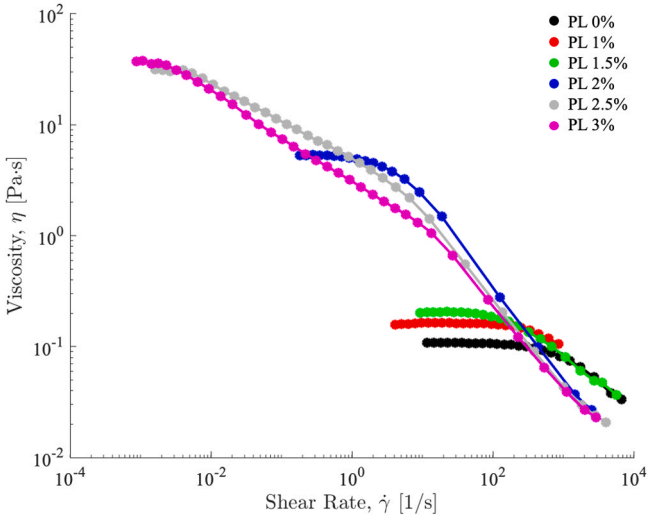

Fig. 1. Flow curves for 10.7 % w/w KOL (black) dispersion and in the presence of PL at 1 % (red), 1.5 % (green), 2 % (blue), 2.5 % (grey) and 3 % (purple). The dots and the lines represent the experimental data. The experimental error is 2 % on each curve. (For interpretation of the references to color in this figure legend, the reader is referred to the web version of this article.).

We recall that the reciprocal of the consistency index, $1/C$, provides an estimate of the critical shear rate at which the shear thinning behavior occurs, and an increase in C can be related to a strengthening in the dispersion texture and slower entanglement-disentanglement dynamics, as in the case of polymer solutions [69].

The shear relaxation exponent m is close to 1 (the theoretically predicted value for plastic materials), indicating that the catanionic structures undergo a substantial shear-induced alignment [70].

For the samples containing PL at 2.5 and 3 % a polynomial fit was performed since the Cross model did not provide an accurate description of the experimental viscosity data, due to the presence of the two different power law dependencies. A fifth-order polynomial model was used:

$$\log\eta = \sum_{i=0}^{5} A_i \log(\dot{\gamma})^i \quad (2)$$

The fitting curves according to this model are shown in the Supplementary Material (Figure S2), and the extrapolated parameters are listed in Table 1.

The complex flow behavior of the PL 2.5 and 3 % samples can be ascribed to the simultaneous presence of two different populations of catanionic structures, that undergo different disaggregation or disentanglement and alignment processes upon shear rate increase, determining a non-uniform power-law region in the flow curves. A visual inspection of the samples provides further insights about this peculiar behavior (Figure S3 in the Supplementary Material). The presence of PL up to 2 % leads to the formation of transparent, homogeneous and highly viscous dispersions, while upon further PL addition the samples become opaque, indicating the occurrence of an aggregation phenomenon or the formation of a coacervate.

A detailed structural investigation was performed via Confocal Laser Scanning Microscopy (CLSM) on the samples containing 0, 1, 1.5 and 3 % of PL to obtain an overview of the aggregation phenomena in the different PL concentration' regimes. Nile Red was selected as hydrophobic probe to monitor the structural modifications occurring within the lipophilic portion of the KOL micellar aggregates. The CLSM images are reported in Fig. 2.

The CLSM images provide clear visual evidences that support the discussion of the rheological behavior. In the absence of PL (Fig. 2a), the sample appears homogeneous with no macroscopic aggregates, consistent with the relatively low viscosity and Newtonian behavior observed in the flow curve. These results are in good agreement with those obtained via cryo-TEM experiments on sodium oleate water dispersions reported in the literature [42], showing a threadlike micellar structure with aggregate dimensions below 50 nm. In the samples containing 1 % and 1.5 % PL (Figure S4 in the Supplementary Material), no significant changes are observed compared to the pure KOL dispersion. At 3 % PL (Fig. 2b and c), bright, densely packed domains are evident, indicating the formation of larger, more complex aggregates and phase-separated structures. This morphological change correlates well with the marked increase in viscosity and the emergence of dual power-law behavior in the flow curves at higher PL concentrations. The appearance of such heterogeneous microdomains likely reflects the coexistence of multiple aggregation regimes, confirming the transition from a homogeneous entangled micellar network to a more complex, possibly coacervate-like system. The three-dimensional reconstruction of the z-stacked CLSM images reported in Fig. 2d highlights the presence of aggregate populations with different morphologies, including elongated features and more compact globular structures with characteristic dimensions on the order of tens of micrometers. A semiquantitative image analysis performed on selected CLSM sections indicates that the elongated structures

Table 1
Zero-shear viscosity η_0, shear relaxation exponent *m*, consistency index *C* obtained by fitting the experimental viscosity data with the Cross model, and the coefficients A_0, A_1, A_2, A_3, A_4, and A_5 obtained from the polynomial model.

	PL Conc. (%)	η_0 (Pa·s)	C (s)	m			
Cross Model	0	0.110	$3.88{\cdot}10^{-4}$	1.05			
	1	0.161	$1.47{\cdot}10^{-3}$	0.93			
	1.5	0.21	$1.53{\cdot}10^{-3}$	0.89			
	2	5.95	0.17	0.94			
Polynomial Model		A_0	A_1	A_2	A_3	A_4	A_5
	2.5	$6.95{\cdot}10^{-1}$	$-3.67{\cdot}10^{-1}$	$-7.23{\cdot}10^{-2}$	$-4.42{\cdot}10^{-2}$	$4.37{\cdot}10^{-5}$	$3.69{\cdot}10^{-3}$
	3	$5.00{\cdot}10^{-1}$	$-3.65{\cdot}10^{-1}$	$-3.08{\cdot}10^{-2}$	$-4.06{\cdot}10^{-2}$	$-1.62{\cdot}10^{-3}$	$2.94{\cdot}10^{-3}$

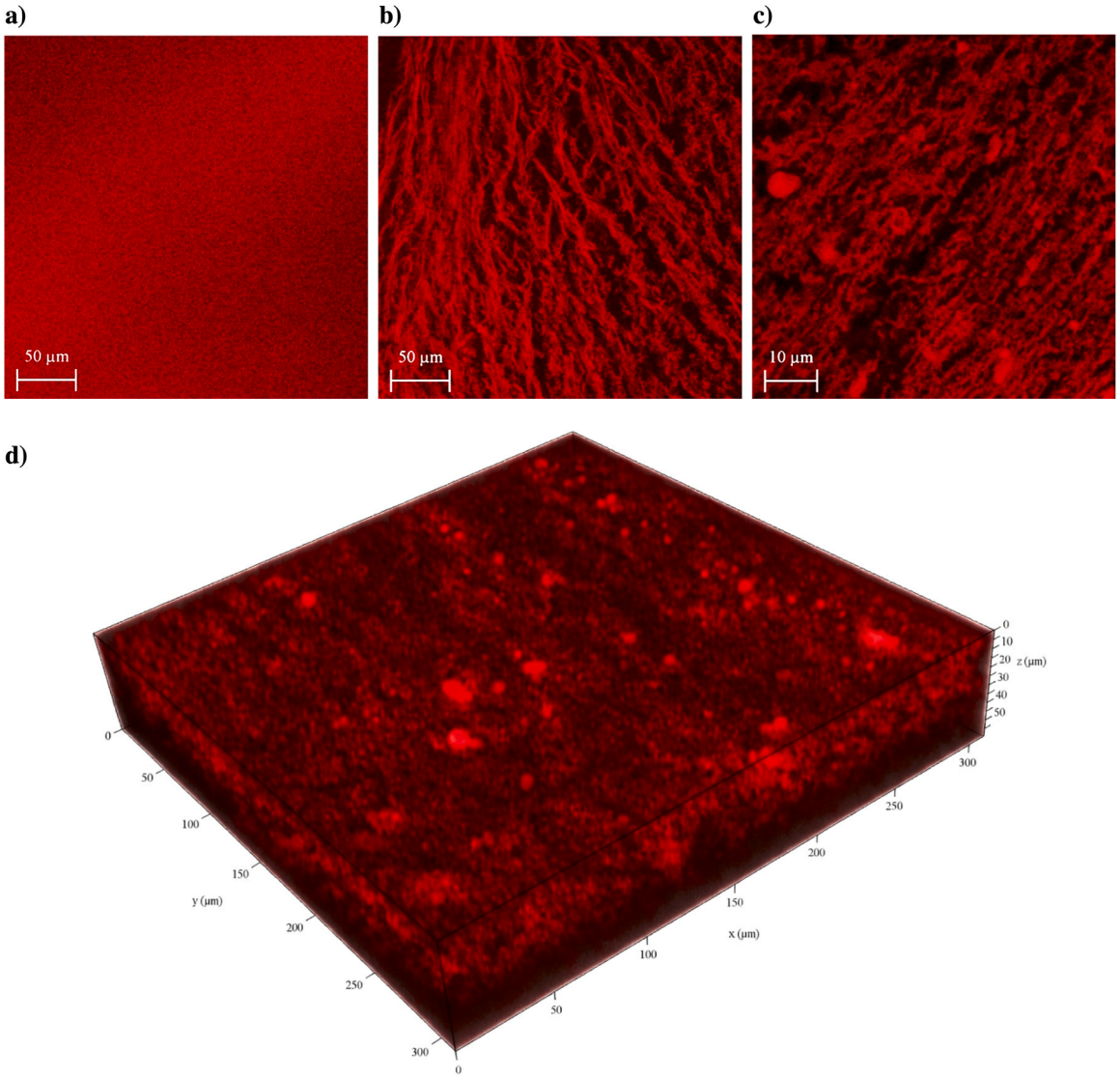

Fig. 2. Confocal laser scanning microscopy images for KOL sample with no added PL (a) and in the presence of 3 % PL with two different magnifications (b and c). Panel d) shows the 3D reconstruction of the z-stacked images for the 3 % KOL-PL sample.

define a porous network characterized by pore areas in the range of approximately 100–500 μm^2, while the estimated areas for globular aggregates show values between 2 and 70 μm^2, with an average value of about 20 μm^2. Although the presence of overlapping micellar layers prevents a complete quantitative analysis, these estimates are consistent with the heterogeneous mesoscale organization that emerges at high PL concentration.

Assuming that in the PL concentration range comprised between 0 % and 2 % no phase transition occurs in our systems, a time-cosolute concentration superposition (TCCS) approach is applied in order to obtain the viscosity master curve and analyze the concentration dependence of the transient viscosity data.

A viscosity master curve is shown in Fig. 3, while the values for the horizontal ($a_{T\text{-}PL}$) and vertical ($b_{T\text{-}PL}$) shift factors are listed in Table 2. The *T* subscript indicates the transient character of the viscosity data. PL concentration of 2 % is arbitrarily selected as reference value for the study of the concentration scaling, analogously to the case of polymer solutions [71].

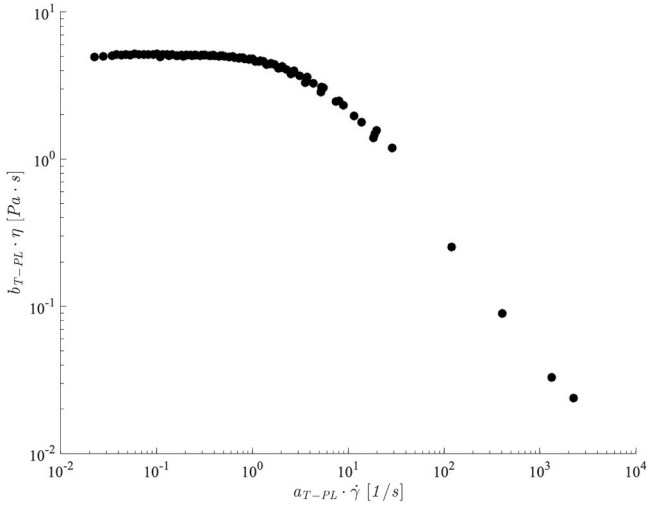

Fig. 3. Viscosity master curve at PL 2 % as reference. The black dots represent the merged master curve.

Table 2
Horizontal ($a_{T\text{-}PL}$), vertical ($b_{T\text{-}PL}$) shift factors for KOL-PL systems.

PL Concentration (%)	$a_{T\text{-}PL}$	$b_{T\text{-}PL}$	$1/b_{T\text{-}PL}$
0	$3.11 \cdot 10^{-3}$	50.00	$2.00 \cdot 10^{-2}$
1.0	$5.03 \cdot 10^{-3}$	33.01	$3.03 \cdot 10^{-2}$
1.5	$1.43 \cdot 10^{-2}$	2.61	$3.85 \cdot 10^{-1}$
2.0	1.00	1.00	1.00

The experimental curves are well superimposed to a single master curve that covers seven decades of shear rates values. By fitting the variations of the shift factors upon PL concentration a power law dependence for $a_{T\text{-}PL}$ and $b_{T\text{-}PL}$ emerges as follows:

$$a_{T-PL} \propto {c_{PL}}^{14.8 \pm 0.4}$$

$$1/b_{T-PL} \propto {c_{PL}}^{11.3 \pm 0.8}$$

where c_{PL} is the PL concentration.

If we consider the horizontal and vertical shift factors as a reduced shear rate (or equivalently a characteristic time λ, with $a_{T-PL} = 1/\dot{\gamma} \approx \lambda$) and a reduced viscosity ($b_{T-PL} = 1/\eta$), respectively, their scaling exponents with the PL concentration can be compared to the power law exponents that can be found for characteristic times and zero-shear viscosities obtained by fitting the experimental data.

In a recent work Berzin and Vergnes [72] observed that in a series of polypropylene homo- and co-polymers the horizontal and the vertical shift factors obtained from the superposition of the viscosity data obeyed power laws as a function of the polymer molecular weight. The same power law dependence was found also for the Newtonian viscosity and the characteristic time estimated from the fitting of the viscosity data with the Carreau–Yasuda model. The exponents for the horizontal and vertical shift factors were very close to the values obtained for the characteristic time and viscosity respectively.

Following a similar approach, the zero-shear viscosity η_0, and the consistency index C obtained from the Cross model are fitted upon the PL concentration. Both parameters follow power law correlations with the PL concentration (c_{PL}) given as:

$$C \propto {c_{PL}}^{14.5 \pm 0.7}$$

$$\eta_0 \propto {c_{PL}}^{11.6 \pm 0.8}$$

The exponent values for C and η_0 are in good agreement to those obtained for $a_{T\text{-}PL}$ and $1/b_{T\text{-}PL}$ respectively, indicating that the superposition approach can be extended to the case of catanionic systems based on potassium oleate and ε-polylsysine to effectively describe their viscous behavior as a function of shear rate and cosolute (PL) concentration. The success of the superposition provides also the confirmation that at constant temperature the concentration ratio between the two oppositely charged polyelectrolytes controls the viscous flow, but its effect on the system structure is negligible.

Other interesting insights can be obtained by plotting η_0 as a function of the PL concentration c_{PL} in semi-log coordinates for the full set of samples (Fig. 4). The values of zero-shear viscosity for samples containing PL at 2.5 and 3 % were estimated from the experimental viscosity data in the low shear region, where a narrow plateau can be detected.

Three distinct regimes can be observed: when the PL concentration is lower than 1.5 % the viscosity is relatively low (Region 1), then upon PL addition the viscosity steeply increases by two orders of magnitude (Region 2). This transition is related to the growth and overlap of cylindrical micelles, that gives rise to an entangled wormlike micellar network [73]. A similar trend was reported by Koshy et al. [74] in the case of sodium oleate-cetyltrimethylammonium bromide catanionic mixtures. The concentration of 1.5 % can be considered the crossover concentration c^* for the catanionic micelles, which is useful to mark out the transition from the dilute to the semidilute (entangled) regime.

In Region 2, the zero-shear viscosity shows a power-law dependency of ${c_{PL}}^{9.9 \pm 1.2}$: a similar exponent was reported for the first time by Molchanov and coworkers for a wormlike micellar solution of a C22-tailed surfactant in the presence of KCl [75]. The value of the exponent is remarkably high if compared to the theoretical value of 5.25 predicted for worm micelles (and equilibrium polymers) [76], or to the experimental values obtained for other WLM systems [77–79]. This effect can be ascribed to a reduced screening of the negative surface of KOL micelles by the positively charged aminoacidic residues on PL [75].

In Region 3 the zero-shear viscosity shows a different trend, slightly increasing with the PL concentration from 2.5 % to 3 %. The change in the slope (and eventually a decrease in η_0 values after a maximum) is usually associated to the formation of branched and/or interconnected structures, where the temporary junctions make the tridimensional network less rigid thanks to the sliding of branch joints along the micellar cylinder [41,80]. In mixed catanionic surfactants' systems cryo-TEM experiments evidenced that the decrease in the zero-shear viscosity after reaching a maximum can be related also to a decrease in the mean contour length of the worms [81]. We recall that for PL concentrations of 2.5 and 3 % the samples become opaque, suggesting a structural modification within the micellar network which is corroborated by the flow curve profiles and CLSM experiments.

To get a deeper insight into the role of the intermolecular interactions between KOL and PL upon the addition of the polyelectrolyte, ATR-FTIR analysis was performed on the oleate-based dispersions at the different PL concentrations. The spectra obtained for the KOL-PL

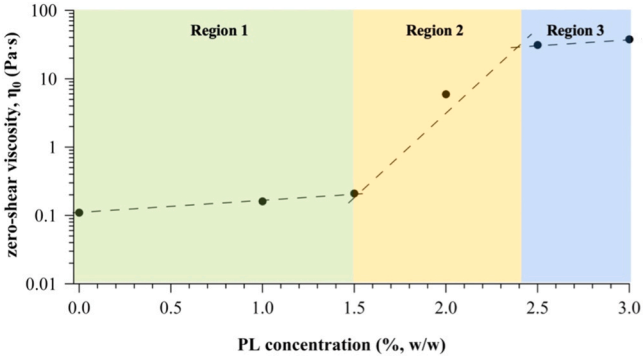

Fig. 4. Zero-shear viscosity as a function of the PL concentration. The dashed lines are guidelines for the eye.

systems and for the pristine KOL and PL water dispersions are shown in Figure S5 and S6 in the Supplementary Material. The spectrum of pure water recorded in the same experimental conditions was subtracted to suppress the bands from free bulk water molecules and highlight the signals arising from the surfactant, the polyelectrolyte and the hydration water, which are organized in clusters and/or layers on the macromolecular surfaces.

For all the investigated samples, intense absorption bands are observed in the 2800–3000 cm^{-1} region, which are assigned to the symmetric (~2850 cm^{-1}) and asymmetric (~2920 cm^{-1}) stretching vibrations of the aliphatic $–CH_2$ groups of the oleate chains. In the 3100–3600 cm^{-1} region, the spectra exhibit a broad composite band primarily arising from the stretching vibrations of water molecules in the hydration shell of KOL aggregates and ε-polylysine chains, and participating in hydrogen bonds (HB). Three distinct contributions are clearly visible, centered at approximately 3220, 3310, and 3400 cm^{-1} . The contributions near 3310 and 3400 cm^{-1} can be attributed to water molecules coordinated through two or three hydrogen bonds in asymmetric structures, while the band at ~3220 cm^{-1} is associated to hydration water molecules close to micellar and polyelectrolyte's surfaces and involved in strong and symmetrical HB [82]. Additionally, a high-frequency shoulder at about 3600 cm^{-1} can be observed. This signal is attributed to weakly hydrogen-bonded O–H groups [83].

The contribution centered at 3310 cm^{-1} remains basically unchanged after PL addition at different concentrations, whereas the peaks at 3220 and 3400 cm^{-1} exhibit a more peculiar behavior (Figure S7 in the Supplementary Material). The ratio between the absorption maxima at 3220 and 3400 cm^{-1} (Abs_{3220}/Abs_{3400}) steeply increases upon addition of 1 % PL, followed by a progressive decrease with further increases in PL content. At 2.5 % PL, the ratio between the absorbance at 3220 and that at 3400 cm^{-1} (Abs_{3220}/Abs_{3400}) returns approximately to the value observed for the pristine KOL dispersion, and at 3 % PL it drops below the initial value. This trend suggests that for PL concentrations up to 2 % the presence of the polyelectrolyte promotes the formation of stronger and more symmetrical HB, thereby reinforcing the PESC network. Conversely, higher PL concentrations negatively affects the HB arrangement, leading to an increased structural heterogeneity within the hydration shell. These results are in good agreement with the structural rearrangements in the high PL concentration regime observed in the CLSM and rheology experiments. It is worth noting that bands from N–H stretching vibrations of ε-polylysine amine groups are supposed to contribute in this region, but the detection of these peaks is not possible due to the overlap with the more intense absorptions of hydration water molecules.

The spectral region between 1400 and 1650 cm^{-1} shows distinct bands associated to carboxylate (COO^-) stretching vibrations of the oleate headgroups, along with an intense signal centered at 1630 cm^{-1} which is attributed to O-H bending in water molecules [84]. The asymmetric COO^- stretch appears near 1540–1550 cm^{-1} , while the symmetric stretch is observed at 1405 cm^{-1} [85]. The changes in bands' intensities upon the addition of PL may suggest possible complex formation between the anionic oleate and the cationic ε-polylysine, however no clear trends can be detected. Minor bands in the amide region (~1650 and ~1550 cm^{-1}) may also reflect contributions from amide I (C═O stretch) and amide II (N–H bending) modes of polylysine [86],but the overlap with the carboxylate region makes the detailed assignment challenging.

To resolve the complex, overlapping spectral changes and elucidate the sequence of structural rearrangements that occur as the PL concentration increases, two-dimensional correlation spectroscopy (2D-COS) was applied on ATR-FTIR data. The synchronous (Φ) and asynchronous (Ψ) spectra obtained using the increase in PL concentration as external perturbation are shown in Fig. 5.

The analysis of the synchronous (Φ) spectrum first reveals strong positive autopeaks along the diagonal at approximately 3200, 2900, 1570, and 1460 cm^{-1} , confirming that the H-bonding environment and the distinct functional groups of the KOL molecules are all highly sensitive to PL addition. Furthermore, the cross-peaks in the synchronous spectrum show a positive correlation between the KOL headgroups and tail regions ($\Phi(2900, 1550) > 0$; $\Phi(2900, 1400) > 0$), indicating a coherent response within the oleate molecule. In contrast, significant negative cross-peaks appear between the H-bonding region and the KOL bands ($\Phi(3200, 2900) < 0$; $\Phi(3200, 1550) < 0$), highlighting an anti-correlated relationship between the micellar structure and the bulk aqueous/peptide environment upon PL addition.

To elucidate the sensitivity of these IR bands to concentration changes, the asynchronous (Ψ) spectrum was analyzed using the Noda's rule [64]. When the external perturbation is time, this rule determines the sequence of events by combining the signs of the synchronous (Φ) and asynchronous (Ψ) cross-peaks at a given coordinate (ν_1, ν_2). For instance, if $\Phi(\nu_1, \nu_2)$ is positive but $\Psi(\nu_1, \nu_2)$ is negative, the change at ν_2 occurs before ν_1. If $\Phi(\nu_1, \nu_2)$ is negative and $\Psi(\nu_1, \nu_2)$ is positive, the sequence is also $\nu_2 \rightarrow \nu_1$. If the perturbation is a concentration variation as in our case, the asynchronous map provides information about the order of responsiveness or sensitivity to concentration changes.

The application of this rule to the KOL-PL correlation maps reveals a peculiar interaction mechanism between the surfactant and the polyelectrolyte. The KOL carboxylate headgroups (circa 1400 and 1550 cm^{-1}) are the most sensitive moieties, responding first to the increasing PL concentration. This is followed by a response from the less sensitive hydrophobic alkyl tails at 2900 cm^{-1}). The analysis confirms that the rearrangement of the H-bonding network (~3200 cm^{-1}) is the

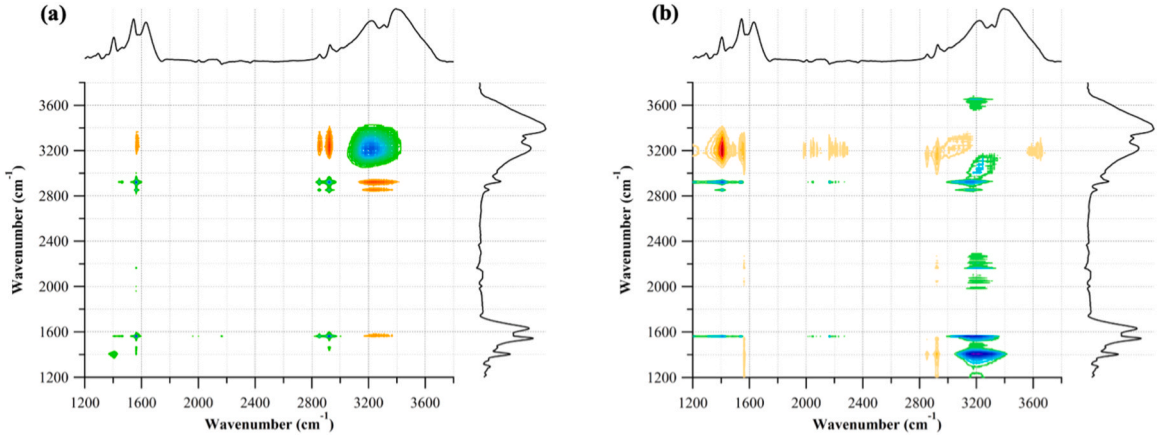

Fig. 5. Synchronous (a) and asynchronous (b) spectra obtained from the ATR-FTIR data on KOL-PL dispersions using PL concentration increase as external perturbation. The orange-red colour scale corresponds to negative values, the green-blue scale indicates positive values.

least sensitive part of the system, taking place only after the initial changes in the headgroup and tail, as evidenced by the negative synchronous (Φ) and positive asynchronous (Ψ) cross-peaks. This sequence provides a molecular-level description of the mechanism suggested by rheology experiments: the primary responsiveness of the headgroups corresponds to the initial exchange between K^+ and PL molecules at the micellar interface, which then triggers the rearrangement of the alkyl tails as the micelles elongate, ultimately leading to the change in the bulk H-bonding network upon the entanglement of these larger structures.

3.2. KOL-PAA system

The flow profiles of the samples containing KOL at 10.7 % and PAA at different concentrations are reported in Fig. 6.

All the samples show a shear-thinning behavior, that becomes more pronounced as PAA concentration increases. The addition of PAA brings about a remarkable increase in the systems' viscosity, suggesting a strong synergistic interaction between the polyacrylate charged chains and the rodlike micelles formed by KOL. The low-molecular weight (M_W = 1200 g/mol) PAA investigated in this work gives rise to a low viscosity solution and exhibits a weak shear-rate dependence at 4.8 % in water (see Figure S1 in the Supplementary Material). Concentrated solutions of other commercially available low-molecular weight PAA show viscosities values ranging from 0.4 to 0.8 Pa·s [87]. Higher molecular weight PAA ($166{\cdot}10^3$ g/mol) solutions show a viscosity of approximately 10–20 mPa·s for a polymer concentration ranging from 0 % to 5 % w/w [88]. Starting from these observations, and considering the relatively low viscosity of the pure KOL dispersion (black curve in Fig. 6), the structuring effect of the PAA addition to KOL micellar solutions becomes evident. PAA has been extensively used as a stabilizer for colloidal systems, as it can adsorb onto the surface of colloidal particles, and due to the high number of carboxyl moieties, it becomes negatively charged when ionized. This results in increased electrostatic repulsion between particles, making them more easily dispersed [89]. Moreover, the polymer chains can extend from the surface providing an additional steric repulsion [90]. In previous works the effect of oppositely charged polyelectrolytes on anionic and cationic wormlike micellar systems was described, highlighting the strengthening of the electrostatic interactions within the mixed polymeric/micellar network, that results in a remarkable viscosity increase [91,92]. To the best of our knowledge only few studies investigated the interaction between PAA and anionic surfactants. Iliopoulos *et al.* [93] observed no viscosity enhancement upon the addition of sodium dodecyl sulfate (SDS) to aqueous solutions of sodium polyacrylate (NaPA), while Maltesh and Somasundaran evidenced a weak polyelectrolyte-surfactant association between PAA and SDS under acidic conditions when the PAA concentration is low [94]. Li *et al.* found that SDS competes for surface sites with NaPA when NaPA is adsorbed on charged TiO_2 particles, displacing some of the bound polyacrylate segments from the surface [95]. To the best of our knowledge, this is the first report of a strong synergic effect between PAA (and more in general, a negatively charged polyelectrolyte) and a WLM system with a negative micellar surface charge. This phenomenon may appear counterintuitive, but there are two main factors that must be carefully addressed. First of all, the effect of the counterion condensation on both micellar and polyelectrolyte surfaces plays a key role in modulating the intermolecular interactions: according to Manning's theory [96] and its more recent interpretation [97], the extent of ion condensation is ruled by the dimensionless linear charge density parameter (ξ), expressed as the ratio between the electrostatic and thermal energies (k_BT):

$$\xi = \frac{q^2}{4\pi\varepsilon_0\epsilon k_B T b} \tag{3}$$

where q, ε_0, ε, k_B, T and b are the elementary charge, the vacuum permittivity, the dielectric constant of water, the Boltzmann constant, the absolute temperature and the average distance between interfacial charges, respectively. In the case of rodlike oleate-based micelles $\xi > 1$, indicating a large counterion condensation on the micellar surface [42]. For polyacrylate aqueous solutions, the calculated value of the linear charge density parameter is 2.83, larger than the critical value of $\xi = 1$ for ion condensation. In the mixed KOL-PAA system a significant fraction of the Na^+ and K^+ counterions are localized near the polymer and micellar surface, leading to a reduction in the electrostatic repulsion between PAA chains and oleate WLMs and promoting their mutual interaction. A similar effect was reported in the case of cationic like-charged polyelectrolyte/surfactant systems [98]. Secondly, hydrogen bonding plays a crucial role in modulating the rheological and phase behavior of the KOL-PAA system. In sodium and potassium oleate water solutions, for pH values ranging from 2 to 10, non-ionized (RCOOH) and anionic ($RCOO^-$) species coexist, and hydrogen bonds stabilize the formation of [R-COO^-···HOOC-R] complexes [41]. On the other hand PAA becomes fully ionized at pH 10, and the ionization degree is essentially independent of its molecular weight [99]. Thus, in mixed KOL-PAA systems (pH 8) intermolecular hydrogen bonds occur between non-ionized and anionic carboxylic moieties located both on oleate micellar surfaces and PAA chains, leading to a synergistic interaction that brings about a remarkable viscosity increase.

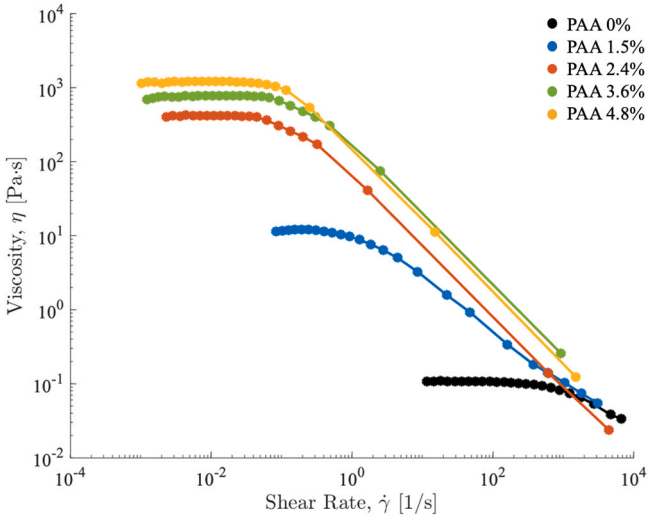

Fig. 6. Flow curves for 10.7 % w/w KOL (black) and in the presence of PAA at 1.5 % (blue), 2.4 % (red), 3.6 % (green) and 4.8 % (orange). The dots and the lines represent the experimental data. The experimental error is 2 % on each curve. (For interpretation of the references to colour in this figure legend, the reader is referred to the web version of this article.).

The flow curves for KOL-PAA dispersions were fitted according to the Cross model (Eq. 1) and the results are listed in Table 3. All the samples show a shear relaxation exponent m around 1, indicating a significant shear-induced alignment, as in the case of entangled WLM in the absence of added polymer.

Following an approach similar to that already used for KOL-PL systems, a time-cosolute concentration superposition is applied to obtain the viscosity master curve and determine the viscosity shift factors. A PAA concentration of 4.8 % is arbitrary selected as reference value for the study of the concentration scaling. Fig. 7 reports the viscosity master curve, while the values for the horizontal ($a_{T\text{-}PAA}$) and vertical ($b_{T\text{-}PAA}$) shift factors are listed in Table 3.

The flow curves can be superimposed to a single master curve that covers nearly eight decades of shear rates, with some discrepancies in the shear thinning region. The horizontal ($a_{T\text{-}PAA}$) and vertical ($b_{T\text{-}PAA}$) shift factors, as well as the zero-shear viscosity η_0 and consistency index C, are fitted according to a power-law relationship as a function of the PAA concentration. The extracted power law exponents are:

Table 3
Horizontal ($a_{T\text{-}PAA}$), vertical ($b_{T\text{-}PAA}$) shift factors, zero-shear viscosity η_0, shear relaxation exponent *m* and consistency index *C* obtained by fitting the experimental viscosity data with the Cross model for KOL-PAA systems.

PAA Concentration (%)	$a_{T\text{-}PAA}$	$b_{T\text{-}PAA}$	$1/b_{T\text{-}PAA}$	η_0 (Pa·s)	C (s)	m
0	$9.01{\cdot}10^{-5}$	$7.75{\cdot}10^{3}$	$1.29{\cdot}10^{-4}$	0.110	$3.88{\cdot}10^{-4}$	1.05
1.500	$8.61{\cdot}10^{-3}$	$1.17{\cdot}10^{2}$	$8.52{\cdot}10^{-3}$	16.06	0.738	0.76
2.400	0.640	2.915	0.343	447.5	2.349	0.97
3.600	0.897	1.577	0.634	799.6	3.083	1.06
4.800	1.000	1.000	1.000	1293.6	4.92	1.05

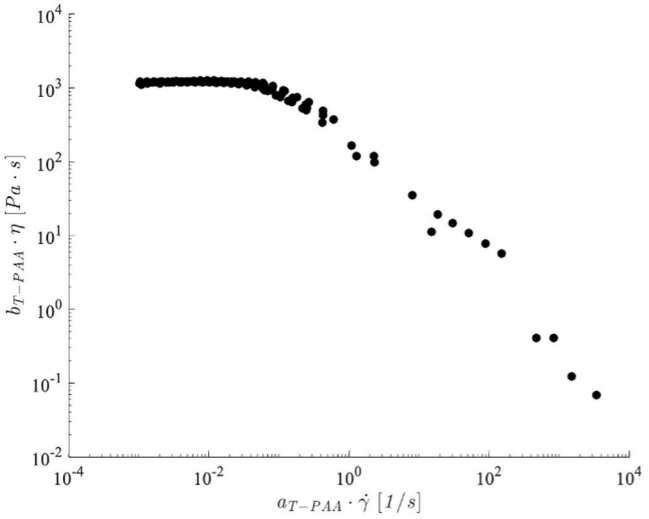

Fig. 7. Viscosity master curve at PAA 4.8 % as reference. The black dots represent the merged master curve.

$a_{T-PAA} \propto c^{1.2\pm0.1}$

$1/b_{T-PL} \propto c^{1.8\pm0.2}$

$C \propto c_{PAA}{}^{1.3\pm0.1}$

$\eta_0 \propto c_{PAA}{}^{1.8\pm0.1}$

The exponents for *C* and η_0 are in good agreement to those obtained for $a_{T\text{-}PAA}$ and $1/b_{T\text{-}PAA}$ respectively. Therefore, the TCCS approach can be successfully extended to the case of the mixed KOL-PAA system, providing an accurate model for the representation of the experimental viscosity data. As in the case of KOL-PL, this method allows also for a reduction of the variables that must be taken into account to describe the viscous behavior of the polymer-WLM system (if compared to Cross or Yasuda-Carreau model for example), since the viscosity can be defined as a function of shear rate, temperature and cosolute concentration.

CLSM analysis was carried out on KOL-PAA samples to explore potential morphological changes induced by the polymer addition. The image recorded at the highest PAA concentration (4.8 %) is reported in the Supplementary Material (Figure S8), as an illustrative example of the system at the upper concentration limit. For all the investigated concentrations the CSLM images display a homogeneous fluorescence signal with no detectable micro- or mesoscale aggregates, suggesting that the micellar structures remain below the optical resolution limit of this technique. The absence of visible large-scale domains or phase-separated regions supports the hypothesis that PAA does not induce macroscopic aggregation or coacervation, but can alter the micellar architecture at the nanoscale—an effect that is not captured by CLSM imaging but is clearly reflected in the rheological behavior.

The viscoelastic properties of mixed KOL-PAA polyelectrolyte systems were investigated by means of oscillatory shear measurements as a function of PAA concentration. Fig. 8 (left panel) shows the storage (G′) and loss (G″) moduli obtained by frequency sweep experiments for the aqueous solutions of potassium oleate in the presence of PAA at different concentrations. The data for the pure polymer solution and for KOL alone are not shown since these two systems do not exhibit viscoelastic response in the investigated frequency and concentration range.

All the samples exhibit a characteristic viscoelastic liquid behavior. At low frequencies the liquid-like behavior predominates (G'' > G'), while at higher frequencies the solid-like elastic behavior prevails (G' > G''). The frequency ω_c at the crossover point when G'=G'' is inversely related to the characteristic relaxation time of the material λ_R. The profiles of the storage and loss moduli reveal a strong concentration dependence. The crossover frequency shows a progressive decrease as PAA concentration increases, similar to those obtained for oleate-based

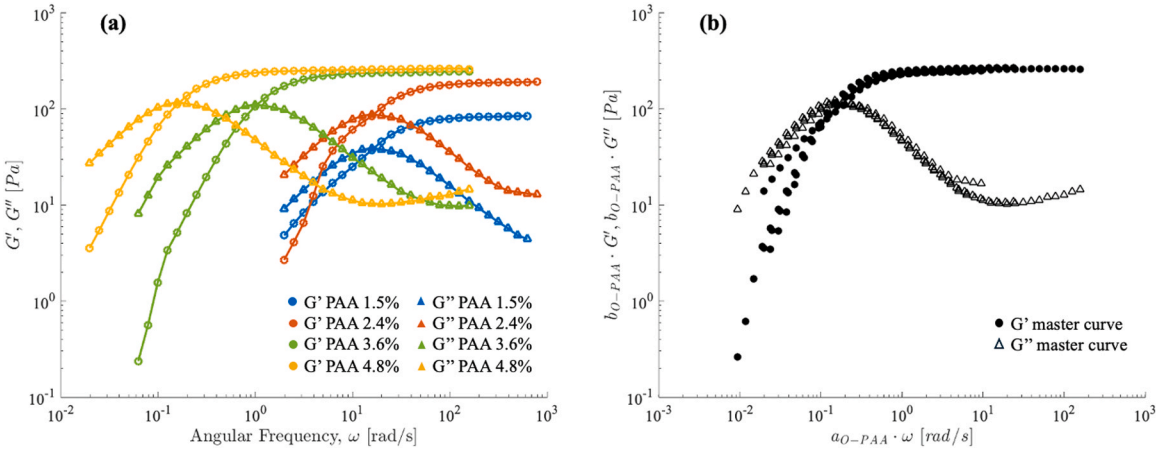

Fig. 8. Left panel (a): storage (circles) and loss (triangles) moduli for 10.7 % w/w KOL dispersions in the presence of PAA at 1.5 % (blue), 2.4 % (red), 3.6 % (green) and 4.8 % (orange). Right panel (b): master curve for the oscillatory data master at PAA 4.8 % as reference. The full circles represent the storage modulus, the empty triangles represent the loss modulus.

WLM in the presence of different salt concentrations [41], suggesting a slower relaxation dynamics (i.e. longer relaxation times) due to a more interconnected structure. This effect is observable also in the trend of the dynamic moduli G' and G'', that increase as PAA concentration increases. Thus, the overall behavior is mainly determined by the viscoelastic features of KOL wormlike micelles, while PAA acts as a synergistic "modifier" that enhances the rheological properties of the mixed system. This effect can be ascribed to the formation of a common network where the polymer chains connect different wormlike structures [100].

The viscoelastic behavior of entangled wormlike networks can be described by the Maxwell model for viscoelastic fluids with a characteristic relaxation time λ_R, according to the following equations [101]:

$$G' = G_0 \frac{\omega^2 \lambda_R^2}{\omega^2 \lambda_R^2 + 1} \quad (4)$$

$$G'' = G_0 \frac{\omega \lambda_R}{\omega^2 \lambda_R^2 + 1} \quad (5)$$

where G_0 is the elastic modulus extrapolated to infinite frequency (the plateau modulus). The values obtained for G_0 and λ_R at different PAA concentrations are listed in Table 4. The detailed discussion of the theoretical background and the experimental procedures can be found in reference [41] and will not be reported here.

Similarly to the TCCS approach for viscosity data, the concentration dependence of the linear viscoelastic properties of KOL-PAA system was investigated by applying the same procedure to the data shown in Fig. 8. The time-cosolute concentration shifting of the oscillatory data implies the multiplication of the dynamic moduli G' (ω, c_{PAA}), G'' (ω, c_{PAA}) with the vertical shift factor $b_{O\text{-}PAA}$ and a multiplication of the angular frequency with the horizontal shift factor $a_{O\text{-}PAA}$ as follows:

$$b_{O-PAA} G'(a_{O-PAA}\omega, \quad c_{PAA}) = G'_{ref} \quad (6)$$

$$b_{O-PAA} G''(a_{O-PAA}\omega, \quad c_{PAA}) = G''_{ref} \quad (7)$$

Where G'_{ref} and G''_{ref} are the storage and the loss modulus for the reference concentration, respectively. The O subscript indicates the oscillatory character of the frequency sweep data. The viscoelastic master curve is shown in Fig. 8, while the values for the horizontal ($a_{O\text{-}PAA}$) and vertical ($b_{O\text{-}PAA}$) shift factors are listed in Table 4.

At high frequencies, in the Rouse dynamic regime, the linear viscoelastic data are well superimposed, while some discrepancies occur in the low-frequency region, that corresponds to the terminal entanglement dynamic regime. This effect has been frequently observed in polymer solutions [71,102,103]. As reported by Li and coworkers [61] the superposition discrepancies in other dynamics at different time and length scales do not affect the dynamics under consideration. The dynamic scaling theory [104,105] predicts that the characteristic timescales of Rouse dynamics are distinctly different from those of entanglement dynamics. Although the profile of the superimposed master curve is not perfect, the horizontal and vertical shift factors can be fitted according to a power law concentration scaling. The concentration scaling of $a_{O\text{-}PAA}$ can be related to the concentration scaling of Rouse characteristic relaxation time λ_R, since the superposition is performed in the Rouse dynamic regime. The concentration dependence of $1/b_{O\text{-}PAA}$ can be compared to the concentration scaling of the plateau modulus G_0, similarly to the case of polymer solutions [106]. The results show that:

$$a_{O-PAA} \propto c_{PAA}^{6.6\pm0.2}$$

$$1/b_{O-PL} \propto c_{PAA}^{0.7\pm0.3}$$

$$\lambda_R \propto c_{PAA}^{6.4\pm0.3}$$

$$G_0 \propto c_{PAA}^{0.8\pm0.3}$$

The scaling exponents are in good agreement with the coefficients obtained with the time-cosolute concentration superposition approach. For this reason TCCS can be considered a very powerful tool to estimate the concentration scaling of linear viscoelastic properties (and steady shear viscosity data) of these systems. This method allows for the construction of a rheological "map" that extends the range of accessible data (not limited to the experimental ones) and for the prediction of the rheological behavior at arbitrarily selected cosolute concentrations, within the range of validity of the superposition approach. Moreover, the existence of different dynamic mechanism can be determined by applying a TCCS shifting, as evidenced before in the case of Rouse and entangled dynamics. To the best of our knowledge this is the first work that demonstrates the efficacy of the time-concentration superposition on complex fluids like mixed polyelectrolyte systems based on wormlike micelles.

A brief note about the complex shear viscosity (η^*) derives from the calculation of measurements η^*. The results for the KOL-PAA samples at different PAA concentration are reported in Figure S9 in the Supplementary Material, along with the experimental shear data. By comparing the η^* profiles with the steady shear data it is evident that the Cox-Merz rule does not hold for the KOL-PAA mixed systems, since major inconsistencies occurs between the oscillatory and steady shear data. The validity of this principle was confirmed for polymer melts and solutions [107], but in the case of gels, pastes and colloidal dispersions significant deviations were observed due to the occurrence of intermolecular interactions that lead to the formation of complex structures and aggregates [108]. In WLM systems the formation of a multiconnected, entangled network results in a departure from the Cox-Merz rule both in the low and high frequency regime [109]. For this reason, complex viscosity was not considered in the study of the concentration scaling of horizontal and vertical shift factors (we recall that the scaling of η^* is equivalent to the scaling of the $b_{O\text{-}PAA}/a_{O\text{-}PAA}$ ratio).

To elucidate the effect of PAA addition on the intermolecular interactions between the surfactant micelles and the polymer chains ATR-FTIR measurements were carried out. The spectra obtained for the KOL-PAA systems and for the pristine PAA water dispersion after the subtraction of pure water spectrum are reported in Figure S6 and S10 in the Supplementary Material.

For all the samples the broad O–H stretching band (3100–3600 cm^{-1}) shows three main contributions centered at approximately 3220, 3310, and 3400 cm^{-1} along with a shoulder at about 3600 cm^{-1} , reflecting the different populations of hydrogen-bonded water at the surfactant–polymer interface. The addition of PAA affects the intensity of these contributions, however a specific trend related to the increasing polymer concentration is not clearly detectable. The 2800–3000 cm^{-1} region displays the characteristic oleate signals at ~2850 and ~2920 cm^{-1} which are assigned to the symmetric and asymmetric stretching vibrations of the aliphatic $–CH_2$ groups respectively. The contribution of PAA to these bands is negligible, as shown in Figure S4 in the Supplementary Material. In the spectral region between 1400 and 1650 cm^{-1} the intense signal centered at 1630 cm^{-1} is attributed to the O–H bending mode in water molecules, while the bands at ~1550 cm^{-1} and ~1400 cm^{-1} are associated to the asymmetric and symmetric COO^- stretching vibrations of the oleate headgroups and PAA

Table 4
Horizontal ($a_{O\text{-}PAA}$), vertical ($b_{O\text{-}PAA}$) shift factors, plateau modulus G_0 and relaxation time λ_R obtained for the KOL-PAA systems.

PAA Concentration (%)	$a_{O\text{-}PAA}$	$b_{O\text{-}PAA}$	λ_R (s)	G_0 (Pa)
1.500	0.011	2.91	0.386	83
2.400	0.013	1.30	0.398	186
3.600	0.151	1.11	6.31	240
4.800	1.000	1.000	39.81	262

moieties. The intensities of the COO^- bands increase upon PAA addition, reflecting the growing contribution of polymer carboxylic/carboxylate groups and their interactions with oleate headgroups and the hydration shell.

To establish the order of sensitivity of different molecular groups to the increasing PAA concentration, two-dimensional correlation spectroscopy (2D-COS) was performed. The resulting synchronous and asynchronous contour plots are shown in Fig. 9.

In the synchronous spectrum, strong positive autopeaks are visible on the diagonal in the H-bonding region (~3300 cm^{-1}), the aliphatic C-H stretching region (~2900 cm^{-1}), and the carboxylate region (~1550–1400 cm^{-1}). This confirms that all these domains are highly sensitive to the addition of PAA. The off-diagonal cross-peaks reveal a positive correlation between the alkyl C-H bands and the COO^- bands, indicating a coherent response within the oleate micellar structure. Conversely, strong negative cross-peaks correlate both the C-H and COO^- bands to the H-bonding region, suggesting that the structural changes within the micelles and the modifications in the surrounding water network occur in opposite directions upon PAA concentration increase.

The analysis of the synchronous (Φ) and asynchronous (Ψ) cross-peaks according to Noda's rule reveals a distinct sequence of events as PAA concentration increases. Specifically, the negative signs of both Φ and Ψ cross-peaks between the H-bonding region and the KOL bands establish the water network as the most sensitive component, responding before any part of the micelle. Furthermore, the positive Φ and negative Ψ cross-peaks between the KOL's functional groups show that the carboxylate headgroup is more sensitive than the alkyl tail. This sequence suggests an "outside-in" mechanism: the addition of PAA first modifies the hydration water structure and the HB network, which then triggers a response at the micelle's polar surface, and this change finally propagates into the hydrophobic core.

The 2D-COS analysis reveals different interaction mechanisms between the KOL micellar system and the two polymers, polyacrylic acid and polylysine. The order of responsiveness to the increasing polyelectrolyte concentration points to distinct initial interaction sites driven by the specific chemical nature of each cosolute. The opposite mechanisms can be attributed to the different electrostatic nature of PAA and PL. PAA is an anionic polymer approaching the anionic micellar surface: the interaction is likely mediated by counterions in solution and hydrogen bonding, which explains why the -OH groups respond first. PL is polycationic and a direct electrostatic attraction occurs between the positively charged aminoacidic residues and the negatively charged COO^- headgroups of the KOL micelles. This interaction leads to the identification by 2D-COS analysis of the carboxylate groups as the most sensitive moities. The binding of PL to the micelle surface is the primary event that triggers all following changes. These results demonstrate that 2D-COS applied to ATR-FTIR data can provide a molecular-level confirmation of the outcomes obtained via rheological experiments, highligthing how the polymer chemistry drives the interaction pathway.

4. Conclusions

In this work, we investigated the rheological behavior of two polyelectrolyte–wormlike micellar complexes formed by potassium oleate in the presence of either ε-poly-L-lysine or poly(acrylic acid). Steady shear and oscillatory measurements revealed distinct concentration-dependent trends for each system, reflecting the interplay between the oleate micellar structure and the polyelectrolyte molecules of different charge. In KOL-PL systems, a marked increase in viscosity was observed above a critical PL concentration (≈ 1.5 %), with a complex flow behavior emerging at higher concentrations, likely due to the formation of supramolecular or coacervate-like micellar aggregates. CLSM imaging supported these findings, showing the development of microstructured domains at high PL content. The complexation between KOL and PL was confirmed at a molecular level by 2D-COS analysis of FTIR data, which revealed an interaction mechanism initiated by the direct electrostatic binding of the polycationic PL to the anionic KOL headgroups. In contrast, the KOL-PAA mixtures exhibited a strong and progressive enhancement in viscosity and viscoelastic moduli with increasing PAA concentration, despite the absence of visible mesoscale aggregation in CLSM images. This behavior is attributed to nanoscale modifications within the micellar network, consistent with previous cryo-TEM observations [42]. This suggests a complex interaction mechanism, probably driven by counterion condensation and hydrogen bonding—that leads to a strong synergistic effect between the two negatively charged species. Our hypothesis is supported by 2D-COS results on FTIR data, that shows an "outside-in" mechanism where the initial response to increasing polymer concentration occurs in the surrounding H-bonding network before propagating into the micellar structure. To the best of our knowledge, this represents the first reported case of such behavior in wormlike micellar systems with a negative surface charge. Notably, PL and PA water dispersions individually exhibit a liquid-like rheological behavior, confirming that the marked increase in viscosity and elasticity arises exclusively from their cooperative interaction with the oleate micellar network. Furthermore, a time–cosolute concentration superposition (TCCS) approach was successfully applied to model the rheological properties of both KOL-PL and KOL-PAA systems. Unified master curves were built by collapsing the viscosity and oscillatory data across the different concentration ranges, enabling the derivation of concentration-scaling relationships. The agreement between TCCS shift factors and the experimental rheological parameters confirms the

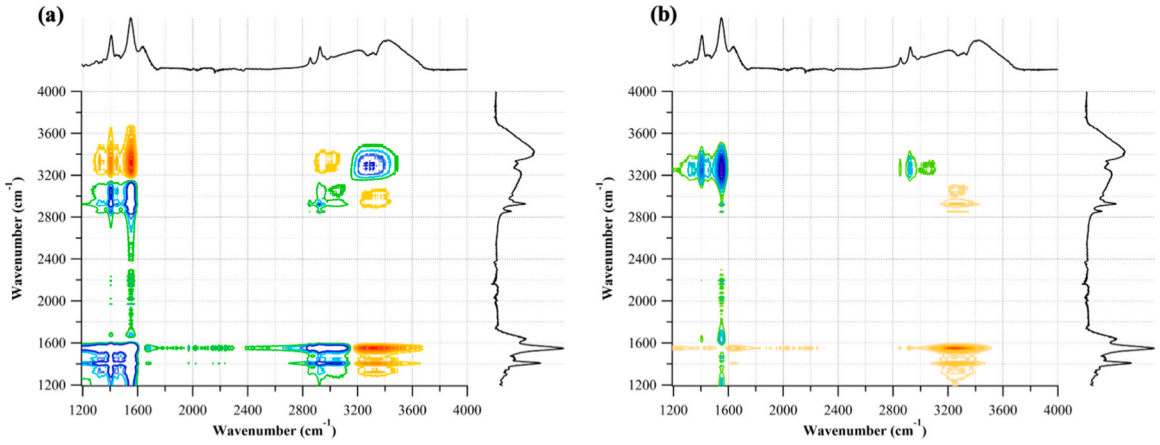

Fig. 9. Synchronous (a) and asynchronous (b) spectra obtained from the ATR-FTIR data on KOL-PAA dispersions using PAA concentration increase as external perturbation. The orange-red colour scale corresponds to negative values, the green-blue scale indicates positive values.

applicability of this method to surfactant–polymer mixtures. This is the first demonstration of TCCS applied to complex fluids comprising mixed polyelectrolytes and wormlike micelles. Our findings highlight the critical role of polymer charge in determining the interaction mechanism and overall flow behavior of polyelectrolyte–micelle complexes, establishing TCCS and 2D-COS as a powerful combination for the quantitative rheological and structural characterization of these complex fluids.

CRediT authorship contribution statement

Mert Acar: Writing – original draft, Visualization, Methodology, Investigation, Formal analysis. **Pierandrea Lo Nostro:** Writing – review & editing, Writing – original draft, Resources, Methodology, Conceptualization. **Duccio Tatini:** Writing – review & editing, Writing – original draft, Software, Methodology, Investigation, Formal analysis, Data curation, Conceptualization. **Alberto Fidi:** Validation, Investigation, Data curation.

Declaration of Competing Interest

The authors declare that they have no known competing financial interests or personal relationships that could have appeared to influence the work reported in this paper.

Acknowledgments

None

Appendix A. Supporting information

Supplementary data associated with this article can be found in the online version at doi:10.1016/j.colsurfa.2026.139621.

Data availability

Data will be made available on request.

References

[1] P. Coussot, 1 - Introduction to the rheology of complex fluids, in: N. Roussel (Ed.), Understanding the Rheology of Concrete, Woodhead Publishing, 2012, pp. 3–22, https://doi.org/10.1533/9780857095282.1.3.
[2] J. Yang, Viscoelastic wormlike micelles and their applications, Curr. Opin. Colloid Interface Sci. 7 (2002) 276–281, https://doi.org/10.1016/S1359-0294(02)00071-7.
[3] Z. Chu, C.A. Dreiss, Y. Feng, Smart wormlike micelles, Chem. Soc. Rev. 42 (2013) 7174–7203, https://doi.org/10.1039/C3CS35490C.
[4] P.M. Visakh, Polyelectrolyte: Thermodynamics and Rheology, in: V.P. M., O. Bayraktar, G.A. Picó (Eds.), Polyelectrolytes: Thermodynamics and Rheology, Springer International Publishing, Cham, 2014, pp. 1–17, https://doi.org/10.1007/978-3-319-01680-1_1.
[5] R.G. Larson, R.G. Larson, The Structure and Rheology of Complex Fluids, Oxford University Press, Oxford, New York, 1999.
[6] C.A. Dreiss, Wormlike micelles: where do we stand? Recent developments, linear rheology and scattering techniques, Soft Matter 3 (2007) 956–970, https://doi.org/10.1039/B705775J.
[7] D.P. Acharya, H. Kunieda, Wormlike micelles in mixed surfactant solutions, Adv. Colloid Interface Sci. 123–126 (2006) 401–413, https://doi.org/10.1016/j.cis.2006.05.024.
[8] S. Ezrahi, E. Tuval, A. Aserin, Properties, main applications and perspectives of worm micelles, Adv. Colloid Interface Sci. 128–130 (2006) 77–102, https://doi.org/10.1016/j.cis.2006.11.017.
[9] D.P. Acharya, D. Varade, K. Aramaki, Effect of temperature on the rheology of wormlike micelles in a mixed surfactant system, J. Colloid Interface Sci. 315 (2007) 330–336, https://doi.org/10.1016/j.jcis.2007.06.025.
[10] L.M. Walker, Rheology and structure of worm-like micelles, Curr. Opin. Colloid Interface Sci. 6 (2001) 451–456, https://doi.org/10.1016/S1359-0294(01)00116-9.
[11] V.S. Molchanov, O.E. Philippova, Stimuli-responsive systems based on polymer-like wormlike micelles of ionic surfactants and their modern applications, Polym. Sci. Ser. C. 65 (2023) 113–127, https://doi.org/10.1134/S1811238223700340.
[12] D. Tatini, M. Raudino, F. Sarri, Light-modulated rheological properties in green innovative formulations, Substantia 6 (2022) 15–26, https://doi.org/10.36253/Substantia-1736.
[13] F. Sarri, D. Tatini, M. Raudino, M. Ambrosi, E. Carretti, P. Lo Nostro, Electro-responsive green gels for lower environmental impact shale gas extraction, Energy Fuels 33 (2019) 2057–2066, https://doi.org/10.1021/acs.energyfuels.8b04321.
[14] Y. Bi, T. Wang, J. Xiao, L. Yu, Wormlike Micelles with photo and pH dual-stimuli-responsive behaviors formed by aqueous mixture of cationic and anionic surfactants, Colloids Surf. A Physicochem. Eng. Asp. 668 (2023) 131441, https://doi.org/10.1016/j.colsurfa.2023.131441.
[15] R.F. López-Santiago, J. Delgado, R. Castillo, Micellar entanglement and its relation to the elastic behavior of wormlike micelle fluids, J. Colloid Interface Sci. 626 (2022) 1015–1027, https://doi.org/10.1016/j.jcis.2022.07.003.
[16] R. Pasquino, R. Castillo, Open issues in the linear and NonLinear rheology of wormlike micelles, Curr. Opin. Colloid Interface Sci. 77 (2025) 101919, https://doi.org/10.1016/j.cocis.2025.101919.
[17] V.S. Meka, M.K.G. Sing, M.R. Pichika, S.R. Nali, V.R.M. Kolapalli, P. Kesharwani, A comprehensive review on polyelectrolyte complexes, Drug Discov. Today 22 (2017) 1697–1706, https://doi.org/10.1016/j.drudis.2017.06.008.
[18] S. Srivastava, M.V. Tirrell, Polyelectrolyte Complexation, in: Advances in Chemical Physics, John Wiley & Sons, Ltd, 2016, pp. 499–544, https://doi.org/10.1002/9781119290971.ch7.
[19] A.F. Thünemann, M. Müller, H. Dautzenberg, J.-F. Joanny, H. Löwen, Polyelectrolyte Complexes, in: M. Schmidt (Ed.), Polyelectrolytes with Defined Molecular Architecture II, Springer, Berlin, Heidelberg, 2004, pp. 113–171, https://doi.org/10.1007/b11350.
[20] C.C.M. Sproncken, B. Gumí-Audenis, S. Foroutanparsa, J.R. Magana, I.K. Voets, Controlling the formation of polyelectrolyte complex nanoparticles using programmable pH reactions, Macromolecules 56 (2023) 226–233, https://doi.org/10.1021/acs.macromol.2c01431.
[21] A. Papagiannopoulos, Current research on polyelectrolyte nanostructures: from molecular interactions to biomedical applications, Macromol 1 (2021) 155–172, https://doi.org/10.3390/macromol1020012.
[22] P.A. Fetin, O.N. Brevnov, M.V. Kadnikov, V.I. Fetina, A.Yu Bilibin, I.M. Zorin, From comb-like polyelectrolytes to polyelectrolyte-surfactant complexes: effect of the length of the aliphatic tail of the counterions on self-organization in solid state, Eur. Polym. J. 152 (2021) 110468, https://doi.org/10.1016/j.eurpolymj.2021.110468.
[23] M. Ishihara, S. Kishimoto, S. Nakamura, Y. Sato, H. Hattori, Polyelectrolyte complexes of natural polymers and their biomedical applications, Polymers 11 (2019) 672, https://doi.org/10.3390/polym11040672.
[24] B. Bolto, J. Gregory, Organic polyelectrolytes in water treatment, Water Res. 41 (2007) 2301–2324, https://doi.org/10.1016/j.watres.2007.03.012.
[25] B.D. Emmanuel, N.Y. Abu-Thabit, N.C. Ngwuluka, 10 - Responsive polyelectrolyte complexes based on natural polysaccharides for drug delivery applications, in: A. S.H. Makhlouf, N.Y. Abu-Thabit (Eds.), Stimuli Responsive Polymeric Nanocarriers for Drug Delivery Applications, 1, Woodhead Publishing, 2018, pp. 267–287, https://doi.org/10.1016/B978-0-08-101997-9.00014-X.
[26] S.M. Lalwani, C.I. Eneh, J.L. Lutkenhaus, Emerging trends in the dynamics of polyelectrolyte complexes, Phys. Chem. Chem. Phys. 22 (2020) 24157–24177, https://doi.org/10.1039/D0CP03696J.
[27] A.F. Thünemann, Polyelectrolyte–surfactant complexes (synthesis, structure and materials aspects), Prog. Polym. Sci. 27 (2002) 1473–1572, https://doi.org/10.1016/S0079-6700(02)00017-5.
[28] K. Kogej, Association and structure formation in oppositely charged polyelectrolyte–surfactant mixtures, Adv. Colloid Interface Sci. 158 (2010) 68–83, https://doi.org/10.1016/j.cis.2009.04.003.
[29] L. Chiappisi, I. Hoffmann, M. Gradzielski, Complexes of oppositely charged polyelectrolytes and surfactants – recent developments in the field of biologically derived polyelectrolytes, Soft Matter 9 (2013) 3896–3909, https://doi.org/10.1039/C3SM27698H.
[30] B. Lindman, F. Antunes, S. Aidarova, M. Miguel, T. Nylander, Polyelectrolyte-surfactant association—from fundamentals to applications, Colloid J. 76 (2014) 585–594, https://doi.org/10.1134/S1061933X14050111.
[31] M. Gradzielski, Polyelectrolyte–surfactant complexes as a formulation tool for drug delivery, Langmuir 38 (2022) 13330–13343, https://doi.org/10.1021/acs.langmuir.2c02166.
[32] S. Llamas, E. Guzmán, F. Ortega, N. Baghdadli, C. Cazeneuve, R.G. Rubio, G. S. Luengo, Adsorption of polyelectrolytes and polyelectrolytes-surfactant mixtures at surfaces: a physico-chemical approach to a cosmetic challenge, Adv. Colloid Interface Sci. 222 (2015) 461–487, https://doi.org/10.1016/j.cis.2014.05.007.
[33] A.L. Kwiatkowski, H. Sharma, V.S. Molchanov, A.S. Orekhov, A.L. Vasiliev, E. E. Dormidontova, O.E. Philippova, Wormlike surfactant micelles with embedded polymer chains, Macromolecules 50 (2017) 7299–7308, https://doi.org/10.1021/acs.macromol.7b01500.
[34] C. Flood, C.A. Dreiss, V. Croce, T. Cosgrove, G. Karlsson, Wormlike Micelles mediated by polyelectrolyte, Langmuir 21 (2005) 7646–7652, https://doi.org/10.1021/la050326r.
[35] N. Khan, B. Brettmann, Intermolecular interactions in polyelectrolyte and surfactant complexes in solution, Polymers 11 (2019) 51, https://doi.org/10.3390/polym11010051.
[36] A.L. Kwiatkowski, H. Sharma, V.S. Molchanov, A.S. Orekhov, A.L. Vasiliev, E. E. Dormidontova, O.E. Philippova, Wormlike surfactant micelles with embedded

polymer chains, Macromolecules 50 (2017) 7299–7308, https://doi.org/10.1021/acs.macromol.7b01500.
[37] A.V. Shibaev, A.V. Makarov, A.I. Kuklin, I. Iliopoulos, O.E. Philippova, Role of charge of micellar worms in modulating structure and rheological properties of their mixtures with nonionic polymer, Macromolecules 51 (2018) 213–221, https://doi.org/10.1021/acs.macromol.7b02246.
[38] H. Sharma, E.E. Dormidontova, Polymer-threaded and polymer-wrapped wormlike micelle solutions: molecular dynamics simulations, Macromolecules 52 (2019) 7016–7027, https://doi.org/10.1021/acs.macromol.9b00974.
[39] X. Xin, G. Xu, Y. Wang, H. Mao, Z. Zhang, Interaction between star-like block copolymer and sodium oleate in aqueous solutions, Eur. Polym. J. 44 (2008) 3246–3255, https://doi.org/10.1016/j.eurpolymj.2008.07.033.
[40] L. Calucci, S. Borsacchi, F. Balzano, R. Volpi, D. Tatini, G. Uccello Barretta, P. Lo Nostro, M. Geppi, Physicochemical characterization of green sodium oleate-based formulations. Part 3. Molecular and collective dynamics in rodlike and wormlike micelles by proton nuclear magnetic resonance relaxation, J. Colloid Interface Sci. 636 (2023) 279–290, https://doi.org/10.1016/j.jcis.2023.01.012.
[41] D. Tatini, M. Raudino, M. Ambrosi, E. Carretti, I. Davidovich, Y. Talmon, B. W. Ninham, P. Lo Nostro, Physicochemical characterization of green sodium oleate-based formulations. Part 1. Structure and rheology, J. Colloid Interface Sci. 590 (2021) 238–248, https://doi.org/10.1016/j.jcis.2021.01.040.
[42] D. Tatini, D. Ciardi, C. Sofroniou, B.W. Ninham, P. Lo Nostro, Physicochemical characterization of green sodium oleate-based formulations. Part 2. Effect of anions, J. Colloid Interface Sci. 617 (2022) 399–408, https://doi.org/10.1016/j.jcis.2022.01.135.
[43] Y. HAMANO, Occurrence, biosynthesis, biodegradation, and industrial and medical applications of a naturally occurring ε-Poly-l-lysine, Biosci. Biotechnol. Biochem 75 (2011) 1226–1233, https://doi.org/10.1271/bbb.110201.
[44] H. Katano, K. Uematsu, C. Maruyama, Y. Hamano, Analytical methods for the detection and purification of ε-Poly-L-lysine for studying biopolymer synthetases, and bioelectroanalysis methods for its functional evaluation, Anal. Sci. 30 (2014) 17–24, https://doi.org/10.2116/analsci.30.17.
[45] I.-L. Shih, M.-H. Shen, Y.-T. Van, Microbial synthesis of poly(ε-lysine) and its various applications, Bioresour. Technol. 97 (2006) 1148–1159, https://doi.org/10.1016/j.biortech.2004.08.012.
[46] J.E. Elliott, M. Macdonald, J. Nie, C.N. Bowman, Structure and swelling of poly (acrylic acid) hydrogels: effect of pH, ionic strength, and dilution on the crosslinked polymer structure, Polymer 45 (2004) 1503–1510, https://doi.org/10.1016/j.polymer.2003.12.040.
[47] T.N. Pashirova, A.B. Afonso, N.V. Terekhova, M.I. Kamalov, P. Masson, E.B. SoutoChapter 5 - Nanogels for drug delivery: physicochemical properties, biological behavior, and in vivo applications, in: M.H. Santana, E.B. Souto, R. Shegokar (Eds.), Nanotechnology and Regenerative Medicine, Academic Press, 2023: pp. 95–131. https://doi.org/10.1016/B978-0-323-90471-1.00005-0..
[48] A. Kausar, Poly(acrylic acid) nanocomposites: design of advanced materials, J. Plast. Film. Sheet 37 (2021) 409–428, https://doi.org/10.1177/8756087920981615.
[49] G. Dalei, S. Das, Polyacrylic acid-based drug delivery systems: a comprehensive review on the state-of-art, J. Drug Deliv. Sci. Technol. 78 (2022) 103988, https://doi.org/10.1016/j.jddst.2022.103988.
[50] L. Alves, B. Lindman, B. Klotz, A. Böttcher, H.-M. Haake, F.E. Antunes, Rheology of polyacrylate systems depends strongly on architecture, Colloid Polym. Sci. 293 (2015) 3285–3293, https://doi.org/10.1007/s00396-015-3715-4.
[51] Y. Park, S. Jin, I. Noda, Y.M. Jung, Continuing progress in the field of two-dimensional correlation spectroscopy (2D-COS), part I. Yesterday and today, Spectrochim. Acta Part A Mol. Biomol. Spectrosc. 281 (2022) 121573, https://doi.org/10.1016/j.saa.2022.121573.
[52] Y. Park, S. Jin, I. Noda, Y.M. Jung, Continuing progress in the field of two-dimensional correlation spectroscopy (2D-COS), part II. Recent noteworthy developments, Spectrochim. Acta Part A Mol. Biomol. Spectrosc. 284 (2023) 121750, https://doi.org/10.1016/j.saa.2022.121750.
[53] Y. Park, I. Noda, Y.M. Jung, Diverse applications of two-dimensional correlation spectroscopy (2D-COS), Appl. Spectrosc. 79 (2025) 36–68, https://doi.org/10.1177/00037028241256397.
[54] H. Zheng, K. Liu, Y. Cui, L. Li, Q. Liu, Y. Men, Synthetic Reversible Fibrous Network Hydrogels Based on a Double-Helical Polyelectrolyte, Angew. Chem. 137 (2025) e202503030, https://doi.org/10.1002/ange.202503030.
[55] Y. Park, I. Noda, Y.M. Jung, Two-dimensional correlation spectroscopy in polymer study, Front. Chem. 3 (2015), https://doi.org/10.3389/fchem.2015.00014.
[56] J. Luo, T. Zhou, X. Fu, H. Liang, A. Zhang, Mechanism in Brill transition of polyamide 66 studied by two-dimensional correlation infrared spectroscopy, Eur. Polym. J. 47 (2011) 230–237, https://doi.org/10.1016/j.eurpolymj.2010.11.017.
[57] Z. Ye, S. Sun, P. Wu, Distinct Cation–Anion Interactions in the UCST and LCST Behavior of Polyelectrolyte Complex Aqueous Solutions, ACS Macro Lett. 9 (2020) 974–979, https://doi.org/10.1021/acsmacrolett.0c00303.
[58] L.-Y. Liu, R.-J. Yang, J. Zhang, G.-M. Gong, Y.-R. Yang, Recent progress in two-dimensional correlation spectroscopy for the environmental detection and analysis, J. Mol. Struct. 1214 (2020) 128263, https://doi.org/10.1016/j.molstruc.2020.128263.
[59] M.E. Muratova, I.V. Mikheev, D.S. Volkov, M.A. Proskurnin, Application of two-dimensional correlation spectroscopy to chemical analysis, J. Anal. Chem. 79 (2024) 339–365, https://doi.org/10.1134/S1061934824040105.
[60] X. Peng, Exploring the validity of time-concentration superposition in glassy colloids: experiments and simulations, Phys. Rev. E 98 (2018), https://doi.org/10.1103/PhysRevE.98.062602.
[61] C.-Q. Li, H.H. Winter, Y.-Q. Fan, G.-X. Xu, X.-F. Yuan, Time–concentration superposition for linear viscoelasticity of polymer solutions, Polymers 15 (2023) 1807, https://doi.org/10.3390/polym15071807.
[62] G.-X. Xu, X.-F. Yuan, Q.-S. Liu, H. Wang, Concentration scaling on linear viscoelastic properties of cellular suspensions and effects of equilibrium phase behavior, Int. J. Mol. Sci. 24 (2023) 4107, https://doi.org/10.3390/ijms24044107.
[63] J. Schindelin, I. Arganda-Carreras, E. Frise, V. Kaynig, M. Longair, T. Pietzsch, S. Preibisch, C. Rueden, S. Saalfeld, B. Schmid, J.-Y. Tinevez, D.J. White, V. Hartenstein, K. Eliceiri, P. Tomancak, A. Cardona, Fiji: an open-source platform for biological-image analysis, Nat. Methods 9 (2012) 676–682, https://doi.org/10.1038/nmeth.2019.
[64] I. Noda, Generalized two-dimensional correlation method applicable to infrared, Raman, and other types of spectroscopy, Appl. Spectrosc. 47 (1993) 1329–1336, https://doi.org/10.1366/0003702934067694.
[65] I. Noda, Y. Ozaki. Two-Dimensional Correlation Spectroscopy – Applications in Vibrational and Optical Spectroscopy, 1st ed., Wiley, 2004 https://doi.org/10.1002/0470012404.
[66] I. Noda, Recent advancement in the field of two-dimensional correlation spectroscopy, J. Mol. Struct. 883–884 (2008) 2–26, https://doi.org/10.1016/j.molstruc.2007.11.038.
[67] F. Dong, J. Hao, R. Luo, Z. Zhang, S. Wang, K. Wu, M. Liu, Identification of the proximate geographical origin of wolfberries by two-dimensional correlation spectroscopy combined with deep learning, Comput. Electron. Agric. 198 (2022) 107027, https://doi.org/10.1016/j.compag.2022.107027.
[68] M.M. Cross, Rheology of non-Newtonian fluids: A new flow equation for pseudoplastic systems, J. Colloid Sci. 20 (1965) 417–437, https://doi.org/10.1016/0095-8522(65)90022-X.
[69] K.W. Ebagninin, A. Benchabane, K. Bekkour, Rheological characterization of poly (ethylene oxide) solutions of different molecular weights, J. Colloid Interface Sci. 336 (2009) 360–367, https://doi.org/10.1016/j.jcis.2009.03.014.
[70] F.E. Antunes, L. Coppola, D. Gaudio, I. Nicotera, C. Oliviero, Shear rheology and phase behaviour of sodium oleate/water mixtures, Colloids Surf. A Physicochem. Eng. Asp. 297 (2007) 95–104, https://doi.org/10.1016/j.colsurfa.2006.10.030.
[71] Y.-Q. Fan, A. Lanzaro, X.-F. Yuan, Universal concentration scaling on rheometric properties of polydisperse and high molecular weight polyacrylamide aqueous solutions, Chin. J. Polym. Sci. 40 (2022) 1432–1440, https://doi.org/10.1007/s10118-022-2757-6.
[72] F. Berzin, B. Vergnes, Time/molecular weight superposition to describe the behavior of controlled-rheology polypropylenes, Polymers 14 (2022) 3398, https://doi.org/10.3390/polym14163398.
[73] V.S. Molchanov, O.E. Philippova, Effects of concentration and temperature on viscoelastic properties of aqueous potassium oleate solutions, Colloid J. 71 (2009) 239–245, https://doi.org/10.1134/S1061933X09020136.
[74] P. Koshy, V.K. Aswal, M. Venkatesh, P.A. Hassan, Unusual scaling in the rheology of branched wormlike micelles formed by cetyltrimethylammonium bromide and sodium oleate, J. Phys. Chem. B 115 (2011) 10817–10825, https://doi.org/10.1021/jp2053986.
[75] V.S. Molchanov, A.V. Rostovtsev, K.B. Shishkhanova, A.I. Kuklin, O. E. Philippova, Strong viscosity increase in aqueous solutions of cationic C22-tailed surfactant wormlike micelles, Fluids 7 (2021) 8, https://doi.org/10.3390/fluids7010008.
[76] S. Ezrahi, E. Tuval, A. Aserin, Properties, main applications and perspectives of worm micelles, Adv. Colloid Interface Sci. 128–130 (2006) 77–102, https://doi.org/10.1016/j.cis.2006.11.017.
[77] A. Khatory, F. Kern, F. Lequeux, J. Appell, G. Porte, N. Morie, A. Ott, W. Urbach, Entangled versus multiconnected network of wormlike micelles, Langmuir 9 (1993) 933–939, https://doi.org/10.1021/la00028a010.
[78] V.S. Molchanov, O.E. Philippova, A.R. Khokhlov, Y.A. Kovalev, A.I. Kuklin, Self-assembled networks highly responsive to hydrocarbons, Langmuir 23 (2007) 105–111, https://doi.org/10.1021/la061612l.
[79] M.E. Cates, S.J. Candau, Statics and dynamics of worm-like surfactant micelles, J. Phys. Condens. Matter 2 (1990) 6869–6892, https://doi.org/10.1088/0953-8984/2/33/001.
[80] S.J. Candau, R. Oda, Linear viscoelasticity of salt-free wormlike micellar solutions, Colloids Surf. A Physicochem. Eng. Asp. 183–185 (2001) 5–14, https://doi.org/10.1016/S0927-7757(01)00535-0.
[81] L. Ziserman, L. Abezgauz, O. Ramon, S.R. Raghavan, D. Danino, Origins of the viscosity peak in wormlike Micellar solutions. 1. Mixed catanionic surfactants. A cryo-transmission electron microscopy study, Langmuir 25 (2009) 10483–10489, https://doi.org/10.1021/la901189k.
[82] M.G. Bridelli, Fourier Transform Infrared Spectroscopy in the Study of Hydrated Biological Macromolecules, in: Fourier Transforms - High-Tech Application and Current Trends, IntechOpen, 2017, https://doi.org/10.5772/66576.
[83] M. Grossutti, J.R. Dutcher, Correlation between chain architecture and hydration water structure in polysaccharides, Biomacromolecules 17 (2016) 1198–1204, https://doi.org/10.1021/acs.biomac.6b00026.
[84] Swarna, S.K. Pattanayek, A.K. Ghosh, Role of hydrogen bond interactions in water–polyol medium in the thickening behavior of cornstarch suspensions, Colloid Polym. Sci. 295 (2017) 1117–1129, https://doi.org/10.1007/s00396-017-4107-8.
[85] K. Saito, T. Xu, H. Ishikita, Correlation between C=O stretching vibrational frequency and p K_a shift of carboxylic acids, J. Phys. Chem. B 126 (2022) 4999–5006, https://doi.org/10.1021/acs.jpcb.2c02193.
[86] S. Jiang, M. Zeng, Y. Zhao, H. Wu, F. Zhang, Nano-complexation of ε-poly-l-lysine with DNA: Improvement of antimicrobial activity under high phosphate

conditions, Int. J. Biol. Macromol. 127 (2019) 349–356, https://doi.org/10.1016/j.ijbiomac.2018.12.110.
[87] ⟨https://www.shokubai.co.jp/cn/wpcn/wp-content/uploads/2022/12/en_products_221216.pdf⟩, (n.d.). ⟨https://www.shokubai.co.jp/cn/wpcn/wp-content/uploads/2022/12/en_products_221216.pdf⟩ (accessed October 28, 2025).
[88] L. Aricov, A. Băran, E.L. Simion, I.C. Gîfu, D.-F. Anghel, V.V. Jerca, D.M. Vuluga, New insights into the self-assembling of some hydrophobically modified polyacrylates in aqueous solution, Colloid Polym. Sci. 294 (2016) 667–679, https://doi.org/10.1007/s00396-015-3825-z.
[89] J. Hierrezuelo, A. Sadeghpour, I. Szilagyi, A. Vaccaro, M. Borkovec, Electrostatic stabilization of charged colloidal particles with adsorbed polyelectrolytes of opposite charge, Langmuir 26 (2010) 15109–15111, https://doi.org/10.1021/la102912u.
[90] D. Deng, V. Boyko, S.M. Pancera, T. Tadros, Rheological investigations on the influence of addition of sodium polyacrylate to titanium dioxide suspensions, Colloids Surf. A Physicochem. Eng. Asp. 389 (2011) 149–157, https://doi.org/10.1016/j.colsurfa.2011.08.036.
[91] M. Gradzielski, Polymer–surfactant interaction for controlling the rheological properties of aqueous surfactant solutions, Curr. Opin. Colloid Interface Sci. 63 (2023) 101662, https://doi.org/10.1016/j.cocis.2022.101662.
[92] V.S. Molchanov, O.E. Philippova, Dominant role of wormlike micelles in temperature-responsive viscoelastic properties of their mixtures with polymeric chains, J. Colloid Interface Sci. 394 (2013) 353–359, https://doi.org/10.1016/j.jcis.2012.11.018.
[93] I. Iliopoulos, T.K. Wang, R. Audebert, Viscometric evidence of interactions between hydrophobically modified poly(sodium acrylate) and sodium dodecyl sulfate, Langmuir 7 (1991) 617–619, https://doi.org/10.1021/la00052a003.
[94] C. Maltesh, P. Somasundaran, Evidence of complexation between poly(acrylic acid) and sodium dodecyl sulfate, Colloids Surf. 69 (1992) 167–172, https://doi.org/10.1016/0166-6622(92)80228-T.
[95] H. Li, C.P. Tripp, Interaction of sodium polyacrylate adsorbed on TiO2 with cationic and anionic surfactants, Langmuir 20 (2004) 10526–10533, https://doi.org/10.1021/la048898j.
[96] G.S. Manning, The molecular theory of polyelectrolyte solutions with applications to the electrostatic properties of polynucleotides, Q. Rev. Biophys. 11 (1978) 179–246, https://doi.org/10.1017/S0033583500002031.
[97] U. Mohanty, B.W. Ninham, I. Oppenheim, Dressed polyions, counterion condensation, and adsorption excess in polyelectrolyte solutions, Proc. Natl. Acad. Sci. U. S. A. 93 (1996) 4342–4344, https://doi.org/10.1073/pnas.93.9.4342.
[98] M.E.A. Bassalah, J.J. Cerdà, T. Sintes, A. Aschi, T. Othman, Complex between cationic like-charged polyelectrolytes/surfactants systems, Eur. Polym. J. 96 (2017) 55–68, https://doi.org/10.1016/j.eurpolymj.2017.08.045.
[99] U. Kim, W.M. Carty, Effect of polymer molecular weight on adsorption and suspension rheology, J. Ceram. Soc. Jpn. 124 (2016) 484–488, https://doi.org/10.2109/jcersj2.15219.
[100] J.A. Shashkina, O.E. Philippova, Y.D. Zaroslov, A.R. Khokhlov, T.A. Pryakhina, I. V. Blagodatskikh, Rheology of viscoelastic solutions of cationic surfactant. Effect of added associating polymer, Langmuir 21 (2005) 1524–1530, https://doi.org/10.1021/la0482756.
[101] H. Rehage, H. Hoffmann, Rheological properties of viscoelastic surfactant systems, J. Phys. Chem. 92 (1988) 4712–4719, https://doi.org/10.1021/j100327a031.
[102] J.A. Carmona, P. Ramírez, M.C. García, J. Santos, J. Muñoz, Linear and non-linear flow behavior of welan gum solutions, Rheol. Acta 58 (2019) 1–8, https://doi.org/10.1007/s00397-018-1120-x.
[103] S. Banik, D. Kong, M.J. San Francisco, G.B. McKenna, Monodisperse Lambda DNA as a Model to Conventional Polymers: A Concentration-Dependent Scaling of the Rheological Properties, Macromolecules 54 (2021) 8632–8654, https://doi.org/10.1021/acs.macromol.0c02537.
[104] P.-G. De Gennes, Scaling Concepts in Polymer Physics, Cornell University Press, Ithaca, NY, USA, 1979.
[105] M. Doi, S.F. Edwards, M. Doi, S.F. Edwards, The Theory of Polymer Dynamics, Oxford University Press, Oxford, New York, 1988.
[106] Y.-Q. Fan, A. Lanzaro, X.-F. Yuan, Universal concentration scaling on rheometric properties of polydisperse and high molecular weight polyacrylamide aqueous solutions, Chin. J. Polym. Sci. 40 (2022) 1432–1440, https://doi.org/10.1007/s10118-022-2757-6.
[107] A.Ya Malkin, Non-Newtonian viscosity in steady-state shear flows, J. NonNewton. Fluid Mech. 192 (2013) 48–65, https://doi.org/10.1016/j.jnnfm.2012.09.015.
[108] B. Zakani, D. Grecov, Yield stress analysis of cellulose nanocrystalline gels, Cellulose 27 (2020) 9337–9353, https://doi.org/10.1007/s10570-020-03429-7.
[109] I.A. Kadoma, C. Ylitalo, J.W. Van Egmond, Structural transitions in wormlike micelles, Rheol. Acta 36 (1997) 1–12, https://doi.org/10.1007/BF00366719.

Glossary

ATR-FTIR: Attenuated Total Reflection Fourier-Transform Infrared Spectroscopy
CLSM: Confocal Laser Scanning Microscopy
COS: Correlation Spectroscopy
2D-COS: Two-Dimensional Correlation Spectroscopy
FTIR: Fourier-Transform Infrared Spectroscopy
HB: Hydrogen Bonds
KOL: Potassium Oleate
NMR: Nuclear Magnetic Resonance
PAA: Poly(acrylic acid)
PEC: Polyelectrolyte Complex
PESC: Polyelectrolyte–Surfactant Complex
PL: ε-Poly-L-lysine
PMT: Photomultiplier Tube
TCCS: Time–Cosolute Concentration Superposition
TEM: Transmission Electron Microscopy
UV-Vis: Ultraviolet–Visible Spectroscopy
WLM: Wormlike Micelle
ϕ / ψ: Synchronous / Asynchronous correlation spectra in 2D-COS
η_0: Zero-Shear Viscosity
G' / G'': Storage Modulus / Loss Modulus
G_0: Plateau Modulus
λ_R: Relaxation Time
ξ: Linear Charge Density Parameter